Host Immune Responses That Promote Initial HIV Spread

K. Wendelsdorf[a], G. Dean[b], Shuhua Hu[c], S. Nordone[b], and H.T. Banks[c]

[a]Virginia Bioinformatics Institute
Virginia Polytechnic Institute and University
Washington Street, MC 0477
Blacksburg, Virginia 24061 USA

[b]Center for Comparative Medicine and Translational Research
Department of Molecular Biomedical Sciences
College of Veterinary Medicine
North Carolina State University
Raleigh, NC 27606 USA

and

[c]Center for Research in Scientific Computation
Center for Quantitative Sciences in Biomedicine
North Carolina State University
Raleigh, NC 27695-8205 USA

July 1, 2011

1. REPORT DATE **01 JUL 2011**	2. REPORT TYPE	3. DATES COVERED **00-00-2011 to 00-00-2011**
4. TITLE AND SUBTITLE **Host Immune Responses That Promote Initial HIV Spread**		5a. CONTRACT NUMBER
		5b. GRANT NUMBER
		5c. PROGRAM ELEMENT NUMBER
6. AUTHOR(S)		5d. PROJECT NUMBER
		5e. TASK NUMBER
		5f. WORK UNIT NUMBER
7. PERFORMING ORGANIZATION NAME(S) AND ADDRESS(ES) **North Carolina State University,Center for Research in Scientific Computation,Department of Mathematics,Raleigh,NC,27695-8212**		8. PERFORMING ORGANIZATION REPORT NUMBER **CRSC-TR10-18**
9. SPONSORING/MONITORING AGENCY NAME(S) AND ADDRESS(ES)		10. SPONSOR/MONITOR'S ACRONYM(S)
		11. SPONSOR/MONITOR'S REPORT NUMBER(S)
12. DISTRIBUTION/AVAILABILITY STATEMENT **Approved for public release; distribution unlimited**		
13. SUPPLEMENTARY NOTES		

14. ABSTRACT

The host in ammatory response to HIV invasion is a necessary component of the innate antiviral activity that vaccines and early interventions seek to exploit/enhance. However the response is dependent on CD4+ T-helper cell 1 (Th1) recruitment and activation. It is this very recruitment of HIV-susceptible target cells that is associated with the initial viral proliferation. Hence, global enhancement of the in ammatory response by T-cells and dendritic cells will likely feed viral propagation. Mucosal entry sites contain inherent pathways, in the form of natural regulatory T-cells (nTreg), that globally dampen the in ammatory response. We created a model of this in ammatory response to virus as well as inherent nTreg-mediated regulation of Th1 recruitment and activation. With simulations using this model we sought to address the net e ect of nTreg activation and its speci c functions as well as identify mechanisms of the natural in ammatory response that are best targeted to inhibit viral spread without compromising initial antiviral activity. Simulation results provide multiple insights that are relevant to developing intervention strategies that seek to exploit natural immune processes: i) induction of the regulatory response through nTreg activation expedites viral proliferation due to viral production by nTreg itself and not to reduced Natural Killer (NK) cell activity; ii) at the same time, induction of the in ammation response through either DC activation or Th1 activation expedites viral proliferation; iii) within the in ammatory pathway, the NK response is an e ective controller of viral proliferation while DC-mediated stimulation of T-cells is a signi cant driver of viral proliferation; and iv) nTreg-mediated DC deactivation plays a signi cant role in slowing viral proliferation by inhibiting T-cell stimulation, making this function an aide to the antiviral immune response.

15. SUBJECT TERMS

16. SECURITY CLASSIFICATION OF:			17. LIMITATION OF ABSTRACT	18. NUMBER OF PAGES	19a. NAME OF RESPONSIBLE PERSON
a. REPORT **unclassified**	b. ABSTRACT **unclassified**	c. THIS PAGE **unclassified**	**Same as Report (SAR)**	**54**	

Abstract

The host inflammatory response to HIV invasion is a necessary component of the innate antiviral activity that vaccines and early interventions seek to exploit/enhance. However, the response is dependent on CD4+ T-helper cell 1 (Th1) recruitment and activation. It is this very recruitment of HIV-susceptible target cells that is associated with the initial viral proliferation. Hence, global enhancement of the inflammatory response by T-cells and dendritic cells will likely feed viral propagation. Mucosal entry sites contain inherent pathways, in the form of natural regulatory T-cells (nTreg), that globally dampen the inflammatory response. We created a model of this inflammatory response to virus as well as inherent nTreg-mediated regulation of Th1 recruitment and activation. With simulations using this model we sought to address the net effect of nTreg activation and its specific functions as well as identify mechanisms of the natural inflammatory response that are best targeted to inhibit viral spread without compromising initial antiviral activity. Simulation results provide multiple insights that are relevant to developing intervention strategies that seek to exploit natural immune processes: i) induction of the regulatory response through nTreg activation expedites viral proliferation due to viral production by nTreg itself and not to reduced Natural Killer (NK) cell activity; ii) at the same time, induction of the inflammation response through either DC activation or Th1 activation expedites viral proliferation; iii) within the inflammatory pathway, the NK response is an effective controller of viral proliferation while DC-mediated stimulation of T-cells is a significant driver of viral proliferation; and iv) nTreg-mediated DC deactivation plays a significant role in slowing viral proliferation by inhibiting T-cell stimulation, making this function an aide to the antiviral immune response.

Key Words: HIV; Innate inflammatory response pathway; Regulatory response pathway; Mathematical model

1 Introduction

Once HIV viremia has peaked in the lymphoid tissue there is little hope of eliminating the virus as this marks systemic spread and establishment of tissue and cellular reservoirs. Research has, therefore, been focussed on what is often referred to as the "window period", the initial two weeks of infection, between exposure to virus and peak viremia.

The vaginal mucosa is the most common site of infection and vaccine strategies focus mainly on promoting inflammation response in this tissue. The immune response at mucosal sites, however, are characterized by the presence of anti-inflammatory factors, such as CD4+ natural regulatory T-cells (CD4+ nTreg), that allow these tissues to generally remain refractory to inflammation. The purpose of this regulation is to allow immune cells of the lungs, GI tract, nasal passages, and genital mucosa to maintain contact with innocuous foreign agents in the external environment without dwelling in a constant state of tissue-damaging hyper-inflammation. In the case of viral infection, a potential effect of anti-inflammatory nTreg is to directly and indirectly dampen key mechanisms of the protective antiviral response, such as DC activation and Natural Killer (NK) cell stimulation. The role that these anti-inflammatory factors play in initial viremia remains unclear. The effect of these interacting pathways on HIV infection is particularly complicated by the fact that the immune cells themselves are permissive hosts for this virus. Relevant questions for infection intervention strategies include *Should one reduce the regulatory response in order to aid antiviral activity, i.e., NK recruitment and activation?* This could unintentionally lead to greater viral proliferation through increased host recruitment and infected Th1 proliferation. Therefore, *Should one enhance the regulatory response to reduce inflammation-associated recruitment and T-cell proliferation?* This strategy could also aid viral proliferation by dampening antiviral NK activity as well as promoting nTreg-derived viremia.

There are a number of models that have been developed in different contexts to answer the general question of whether one should enhance or reduce the immune response in order to better control HIV. For example, a mathematical model of interaction of uninfected CD4+ T cells and the free HIV virus in the plasma is developed in [36] to investigate the effect of immunotherapy with cytokine interleukin-2 (IL-2) on an HIV-infected patient, and it was found that this type of immunotheray can be successful in delaying AIDS progression. While the authors in [16] developed mathematical models of the clinical latency stage of HIV-1 infection with the assumption that HIV-1 infection is limited either by the availability of cells that HIV can infect or by a specific anti-HIV cellular immune response. This assumption is based on the suggestions of various clinical data sets (see the references in [16] for more information) that HIV viral replication is limited by the availability of target cells. The effects of tetanus vaccination on chronically infected HIV

patients were explored in [30] through a mathematical model of interaction between T cells, HIV and other antigen. The study was able to reproduce the general features of the post-vaccination rise in viral load observed in some clinical data sets (see the references in [30] for more information).

In addition, the synergistic interaction between HIV and some other pathogens were investigated by a number of researchers (e.g., [3, 35, 43, 44, 58]). In what follows, we give a brief review of some of this type of work. In [44], mathematical models of population dynamics of T helper cells, HIV, and other pathogens were formulated to address the three facets of the interactions between HIV and other pathogens: enhanced HIV replication due to immune stimulation by other pathogens; modified immune control of other pathogens due to immunological suppression by HIV; and the vicious circle formed by the positive feedback between these effects. This study indicates that there is a threshold number of activated T helper cells above which the immune system is unable to control pre-established pathogens. A mathematical model was created in [35] to describe the interaction of HIV and tuberculosis (TB) with the immune system (T cells and macrophages), and this study indicates that co-infection may indeed play a dramatic role in disease. The authors in [58] proposed a simple mathematical model for the interaction of the immune effector cells with HIV and malaria parasites in an individual host, and showed that HIV infection may increase the risk of malaria and, subsequently, malaria infection promotes the proliferation of HIV.

Recently, a mathematical model describing the dynamics of HIV, CD4+ and CD8+ T cells, and DCs interacting in a human lymph node was formulated and analyzed in [26] to investigate the dual role (enhancing HIV infection process as well as promoting an antiviral immune response) of dendritic cells in immune response to HIV infection. Here we present a study unique in that it explores the net effects of HIV-induced inflammation and subsequent nTreg-induced regulation on initial viral replication and spread to the lymph node specifically in the acute phase, i.e., upon vaginal inoculation. The resulting mathematical model is based on mechanistic knowledge of NK, Th1 and nTreg activation by dendritic cells.

1.1 Innate Inflammatory and Regulatory Pathways

Experimental data regarding the early immune response to HIV upon viral exposure in humans is difficult to obtain as it requires invasive tissue biopsies taken from the gut and genital tissues, the initial site of entry, within a very short time period post-infection. Hence, the current biological model is largely based on data gathered from rhesus macaques infected experimentally with Simian Immunodeficiency Virus (SIV) [2, 24, 47]. Based on

4

these studies, the current biological model for early immune response to SIV and HIV infection are generally assumed to be similar and are described as follows.

Virus enters the vaginal lumen and, within hours, gains access to susceptible immune cells: dendritic cells (DC), CD4+ T-helper cells (Th), and CD4+ natural T-regulatory cells (CD4+ nTreg) in the lamina propria (LP) [47]. This initial, small population of infected cells begins to bud virus approximately 2-4 days post-infection at which point the immune response outlined in Figure 1 is elicited. Specifically, infected cells secrete factors
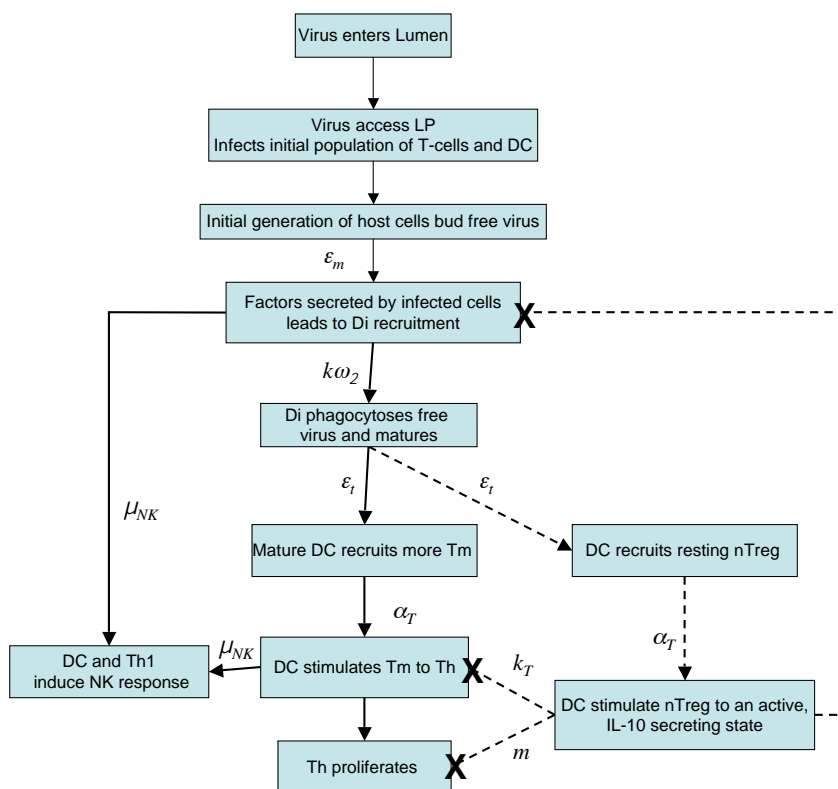
Figure 1: **Immune response to first generation of infected cells** A scheme of the inflammatory (solid lines) and regulatory (dashed lines) included in the model. Arrows are labelled with parameters that determine the rate at which each event occurs.

that trigger a pathway by which monocytes are recruited to the tissue and differentiate into immature dendritic cells (D_i). Free virus, budded from infected cells, is phagocytosed by immature DC leading to their maturation. At this point mature DC secrete factors

5

that recruit resting, or memory, T-helper cells (T_m) and present viral antigen to stimulate these T-cells to a Th1 phenotype [2] rendering them more susceptible to viral infection and promoting their proliferation, allowing enhanced viral replication in infected cells. Both mature DC and inflammatory Th1 then secrete factors such as IL-12 that activate NK cells [6]. NK cells subsequently remove infected cells from the tissue site.

The role of the regulatory pathway in early infection is largely unknown. Yet basic research in various *in vitro* and *in vivo* systems (reviewed in [40] and [51]) have demonstrated mechanisms that we use to construct a biological model of an HIV-dependent regulatory response. In this biological model, resting nTreg, like resting T-helper cells, are recruited and stimulated by mature, antigen-presenting DC via the T-cell receptor. Active nTreg has been shown to carry out numerous regulatory functions. In this biological model the three primary regulatory functions we assign to nTreg are: *i*) contact-dependent deactivation of presenting dendritic cells [48]; *ii*) indirect inhibition of monocyte recruitment through IL-10 secretion, which downregulates expression of inflammatory recruitment factors in surrounding cells [29]; and *iii*) inhibition of T-helper cell proliferation [54]. Like their inflammatory counterparts, CD4+ nTreg is also permissive to HIV infection upon activation [49].

As HIV productively infects the immune cells of these pathways with proliferating T-cells being the most productive hosts, the effect of this normally protective response is not readily predictable. For example, DC uptake of virus and active Th1 presence are critical for NK activation and subsequent removal of virus-producing cells, hindering viral replication. Yet, at the same time, the recruitment of these cells provides a higher concentration of susceptible hosts and their stimulation, inducing viral replication. Indeed, the inflammatory response has been associated with acute viral spread [2]. Given these facts, the nTreg-mediated regulatory pathway could reasonably hinder initial viral propagation by reducing the critical mechanisms of DC-mediated CD4+ T-cell recruitment and activation as well as reduce infected T-cell proliferation.

In short, from the perspective of virus success, nTreg could be equally seen as friend or foe in that it is susceptible to productive viral infection and inhibits inflammation-induced NK activity while, at the same time, inhibiting the inflammatory properties of DCs that are central to the viral lifecycle: T-cell recruitment, activation, and proliferation. Hence, the ultimate effect of nTreg presence on viral success *in vivo* is still unknown.

This work reports the results of simulations carried out to identify specific aspects of the inflammatory and regulatory response pathways that promote and hinder initial viral proliferation from the first generation of infected cells. This work also informs whether regulatory mechanisms could offer new avenues for HIV related interventions as the inflammatory pathway has of other pathogens.

6

Realization of these goals requires a model that captures the dynamics of the true system. This eventually requires rigorous validation using time-course (longitudinal) tissue data that is yet to be found in the literature for the tissue sites of interest, the vaginal mucosa and genital lymph node. An *initial step* toward this goal is reported here in the form of a model that captures the dynamics of the system that is proposed in current literature and is based on the available tissue data. It is worthwhile to note that in developing a mathematical model for any complex biological system there is a balance between complexity and utility (in the context of underlying modeling philosophy, below we shall discuss further this balance between more complex models for which validating data may not currently be available and those which are simple and can be based on only already established accepted mechanisms and data sets). In this paper, we do not try to formulate a model that captures *all* the features of the mucosal immune response as well as all host and viral factors, but rather a model that can capture *many* salient features of the system and for which *some* parameters can be plausibly estimated based on the sparse data available. The model will however involve mechanisms that are still speculative and for which validating data is not yet available. The interested readers can refer to Appendix B for those simplifying assumptions that we made during the modeling reduction processes.

1.2   Some Remarks on Modeling Philosophy

Before proceeding with our efforts in developing a model below, we make some remarks to put our efforts in context of an overall philosophy for the use of mathematical and statistical models in scientific investigations. More detailed discussions on this topic can be found in [15, Chapter 1]. In subsequent developments we will arrive at a fairly complex model for which only a sparse amount of experimental data is available for model validation. (Indeed we are currently able to offer only a partial qualitative validation of our proposed model!) When developing such models it is natural to raise questions of how complex/simple a model one should employ in such investigations. To at least partially answer this, one should consider the underlying reasons that one might give for modeling in science and engineering. The ultimate goal of modeling is not the model itself. Rather modeling is simply a means for providing a conceptual framework in which real systems may be investigated. The modeling process itself is, when properly done, most often an iterative process and often involves efforts over time (and possibly by different research groups). Numerous rationales may be given (to aid in *simplification*, *preciseness*, *formulation of hypotheses*, *design of critical experiments*) but perhaps the most fundamental rationale is that modeling leads to an *organization* of inquiry. Properly done, it tends to polarize one's thinking and aid in posing basic questions concerning what one *does and does not know* for certain about the real system. Whatever the reasons that have been advanced to justify modeling attempts, it is sufficient perhaps to note that the primary goal must be *enlightenment*, that is, *to gain*

7

a better understanding of the real system, and the success or lack thereof of any modeling attempt should be judged with this in mind. Thus, it is not the model itself that is the goal but rather increased understanding of the physical or biological system under investigation. In any modeling attempt, one can seek a simple model that can be validated with existing data and justified in terms of accepted mechanisms. This would result in the simplest model that can explain current theory and data. An alternative approach is to seek a more complex model that stretches our current understanding and poses new questions to be pursued with new conceptual and new experimental investigations. As the reader will see in our subsequent developments below, this latter approach is our choice here. But this will lead to large complex models with a large number of parameters, many of which have not been discussed in the literature. The analysis and attempted validation of such models leads to difficult and ill-posed inverse or parameter estimation problems. We have encountered such difficulties previously, even in earlier HIV infection models (see [4, 9]) and have successfully used an iterative process to alleviate certain aspects of the model analaysis/validation and ill-posedness aspects of the parameter estimation procedures. As explained below, we do that again here.

In related and potentially important research, new methods (illustrated on one of our earlier HIV models in [8]) are currently being developed to formulate and solve such parameter estimation problems. These selection methods involve use of sensitivity functions and information matrices effectively with data sets and complex dynamic models to rank parameters in a model in roughly the order of their importance in the ability of the model to describe (fit) a given data set. As development of these methods matures, they will undoubtedly be of significant value in modeling investigations such as that presented in this paper.

1.3   Model Components

The model describes HIV progression among CD4+ cell populations of conventional T-cells, CD4+ natural T-regulatory cells (CD4+ nTreg), and dendritic cells (DC) as they transition between location and phenotype compartments in response to virus. As such, the only active CD4+ T-helper cells represented are of an inflammatory Th1 phenotype based on cytokine profiles indicating a type 1 response elicited in SIV models [2]. Model variables (compartments) are listed in Table 1 below, and all variables are in units of cells per mL.

Cell populations are compartmentalized by four phenotypes; *i*) resting, generally memory or immature immune cells, denoted with the subscripts 'm' or 'i'; *ii*) active, no subscript; *iii*) infected, denoted with the superscript '*'; *iv*) not infected. These are then further

8

Table 1: Populations represented in the model.

D_i	Immature dendritic cells
D^I	Non-infected active dendritic cells in the GLN
D^{I*}	Infected active dendritic cells in the GLN
D^E	Non-infected active dendritic cells in the LP
D^{E*}	Infected active dendritic cells in the LP
T_m	Non-infected CD4+ Memory T-cells
T_m^*	Latently infected CD4+ Memory T-cells
T^I	Non-infected active CD4+ T helper 1 cells in the GLN
T^{I*}	Infected active CD4+ T helper 1 cells in the GLN
T^E	Non-infected active CD4+ T helper 1 cells in the LP
T^{E*}	Infected active CD4+ T helper 1 cells in the LP
R_m	Non-infected memory CD4+ natural T regulatory cells
R_m^*	Latently infected memory CD4+ natural T regulatory cells
R^I	Non-infected active CD4+ natural T regulatory cells in the GLN
R^{I*}	Infected active CD4+ natural T regulatory cells in the GLN
R^E	Non-infected active CD4+ natural T regulatory cells in the LP
R^{E*}	Infected active CD4+ natural T regulatory cells in the LP

compartmentalized into two tissue sites: *i*) The vaginal lamina propria (LP), more generally termed the *effector* site of the immune response and denoted by the superscript '*E*' ; *ii*) the genital lymph node (GLN), the *inductive* site of the immune response and denoted by the superscript '*I*'.

2 Model Equations

2.1 Dendritic Cells

The scheme for the dynamics of dendritic cells is illustrated in Figure 2. The corresponding
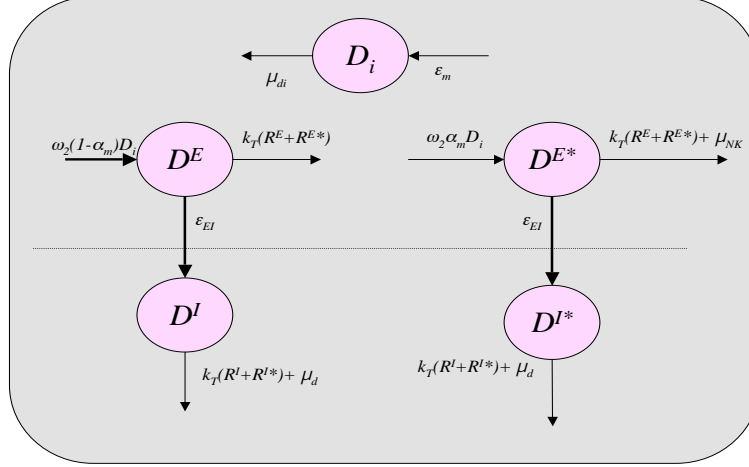
Figure 2: Scheme for dynamics of dendritic cell populations represented.

compartment model for describing its dynamics is given by

$$\dot{D}_i = \varepsilon_m - \mu_{di}(D_i - d_0), \tag{1}$$

$$\dot{D}^I = \varepsilon_{EI}D^E - (k_T(R^{I*} + R^I) + \mu_d)D^I, \tag{2}$$

$$\dot{D}^{I*} = \varepsilon_{EI}D^{E*} - (\mu_d + k_T(R^I + R^{I*}))D^{I*}, \tag{3}$$

$$\dot{D}^E = (1 - \alpha_m)\omega_2 D_i - (\varepsilon_{EI} + k_T(R^E + R^{E*}))D^E, \tag{4}$$

$$\dot{D}^{E*} = \alpha_m\omega_2 D_i - (\varepsilon_{EI} + \mu_{NK} + k_T(R^E + R^{E*}))D^{E*}. \tag{5}$$

where D_i is the concentration of immature dendritic cells, D^I and D^{I*} are, respectively, the concentrations of non-infected and infected activated dendritic cells in the inductive site (GLN), and D^E and D^{E*} are the concentrations of non-infected and infected activated dendritic cells in the effector site (LP). Immature dendritic cells are present in the lamina propria (D_i, Equation (1)) at a constant value of d_0 representing that each D_i that transfers to one of the activated dendritic cell compartments is replaced from an unlimited monocyte pool in the blood [55]. The constant parameter μ_{di} denotes the death rate of the immature dendritic cells. The functional parameter ε_m represents the rate of recruitment of monocytes by inflammatory factors secreted by active immune cells [29] and is a function

of productively infected cells, T^{E*} and D^{E*}, given by

$$\varepsilon_m = c_m \frac{T^{E*} + D^{E*}}{T^{E*} + D^{E*} + R^E}, \tag{6}$$

where c_m is a positive constant. This function is based on the rationale that virus presence induces various inflammatory responses of cells not explicitly represented that promote secretion of recruitment factors and that active CD4+ nTreg secretes IL-10, which can inhibit the expression of these recruitment factors [29]. It is assumed that the IL-10 secretion by productively infected CD4+ nTreg (R^{E*}) cancels out its ability to induce monocyte recruit and is not included in the equation.

Dendritic cells contact and phagocytose free virus at the rate of $\omega_2 = kv_E$. This is the rate of contact with free virus in the effector site where k is the rate of contact between any two cells or cells and virions in both tissue sites and v_E is the amount of free virus in the effector site. Specifically, v_E is a function of productively infected cells given by

$$v_E = N_E(T^{E*} + R^{E*}) + N_D D^{E*}, \tag{7}$$

where N_E is the burst size from T-cells and N_D is the burst size from dendritic cells. Upon phagocytosis all virus is successfully degraded in the presentation process, with a probability of $1 - \alpha_m$, and the cell becomes an active, presenting dendritic cell (D^E, Equation (4)) that is capable of stimulating resting T-cells, promoting NK cytolytic activity, and recruiting resting T-cells from the blood to the tissue. After a period in the LP, corresponding to the migration rate ε_{EI}, the presenting dendritic cells migrate to the GLN joining the D^I population (Equation (2)). Here they can stimulate resting T-cells until they die at a rate of μ_d.

In the case that virions are able to escape degradation and establish infection in a dendritic cell, with a probability of α_m, the cell enters the D^{E*} population (Equation (5)). As with non-infected dendritic cells, those that are infected will migrate to the GLN in the same manner joining the D^{I*} population (Equation (3)).

Active nTreg, that are either infected or not infected, deactivate dendritic cells upon contact rendering them incapable of cytokine secretion or stimulation of resting T-cells [48]. We represent this by removing them from the system upon contact with cells of the active CD4+ nTreg population (R^E, R^{E*}) with the terms $k_T(R^E + R^{E*})$ in Equations (4) and (5) and $k_T(R^{I*} + R^I)$ in Equations (2) and (3), respectively. Here k_T is the contact rate between dendritic cells and nTreg, which was estimated as greater than that between all other cells, k, in agreement with experimental evidence that nTreg have a higher affinity for dendritic cells than do T-helper cells [48].

Similar to all infected cells in the effector site, those of the D^{E*} population may be elimi-

11

nated by cytolytic NK cells at a rate of μ_{NK} given by

$$\mu_{NK} = c_{NK}(1 - e^{-\lambda(D^E + \delta D^{E*} + T^E + T^{E*})}),\tag{8}$$

which is a functional parameter dependent on the concentration of active Th1 and DC based on that fact that IL-12, IL-15, IL-18, IL-21, and interferons (IFN) induce NK cell survival and proliferation, and can promote cytotoxic function. These cytokines are primarily secreted by presenting dendritic cells [6], but IL-12 is also secreted by Th1 T-cells [29]. The constant parameter c_{NK} determines the maximum value μ_{NK} may reach as the concentrations of activated DC and Th1 increase and λ determines the rate at which μ_{NK} rises to this maximum value in proportion to the rise of DC and Th1 concentrations.

Studies have shown that when an immature dendritic cell is infected, its immune functions of antigen presentation and cytokine production may be impaired [22]. Specifically, HIV-infected human DCs *in vitro* have been shown to secrete IL-10 instead of IL-12 and IL-18 and have reduced CD80 expression. However, whether this effect of viral infection occurs *in vivo* and in the acute phase is unknown. To accommodate this possibility the model includes the coefficient δ as seen in Equation (8). This parameter determines the extent to which viral infection impairs the ability of DC to induce NK activation as well as recruit and stimulate T-cells (discussed below). In this context, a value of $\delta < 1$ represents virus-induced inhibition of IL-12 and IL-18 expression reducing the ability of infected DC to recruit and activate NK cells.

NK cells in lymphoid tissue have not been shown to have cytolytic activity *in vivo* [6]. Therefore, those of the D^{I*} population are not considered susceptible to NK-mediated elimination.

2.2 Conventional CD4+ T-cells

The scheme for the dynamics of conventional CD4+ T cells is depicted in Figure 3. The
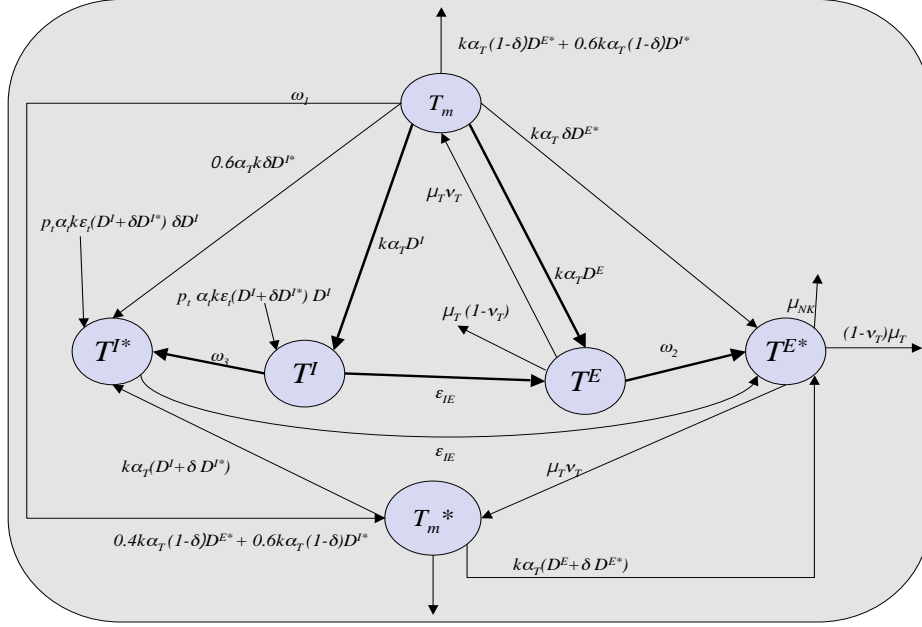
Figure 3: Scheme for dynamics of T-helper cell populations represented.

corresponding compartment model for describing its dynamics is given by

$$\dot{T}_m = \nu_T \mu_T T^E - (k\alpha_T(D^E + D^I + D^{E*} + D^{I*}) + \omega_1)T_m, \tag{9}$$

$$\dot{T}_m^* = \omega_1 T_m + \nu_T \mu_T T^{E*} - (k\alpha_T(D^E + D^I + D^{E*} + D^{I*}))T_m^*, \tag{10}$$

$$\dot{T}^I = p_t k\alpha_t(\varepsilon_t(D^I + \delta D^{I*}))D^I + 0.6 p_t k\alpha_T T_m D^I - (\varepsilon_{IE} + \omega_3)T^I, \tag{11}$$

$$\dot{T}^{I*} = p_t k\alpha_t(\varepsilon_t(D^I + \delta D^{I*}))(\delta D^{I*}) + 0.6 p_t k\alpha_T \delta T_m D^{I*}$$
$$+ \omega_3 T^I + 0.6 p_t k\alpha_T T_m^*(D^I + \delta D^{I*}) - \varepsilon_{IE} T^{I*}, \tag{12}$$

$$\dot{T}^E = \varepsilon_{IE} T^I + 0.4 p_T k\alpha_T T_m D^E - (\mu_T + \omega_2)T^E, \tag{13}$$

$$\dot{T}^{E*} = \varepsilon_{IE} T^{I*} + 0.4 p_T k\alpha_T \delta T_m D^{E*} + \omega_2 T^E$$
$$+ 0.4 p_T k\alpha_T T_m^*(D^E + \delta D^{E*}) - (\mu_T + \mu_{NK})T^{E*}. \tag{14}$$

The model includes a resting T-cell population that represents both *effector* memory T-cells that occupy the LP and *central* memory T-cells that occupy the GLN. This population is compartmentalized into non-infected cells (T_m, (Equation (9)) and latently infected

13

memory T-cells (T_m^*, Equation (10)). All resting T-cells are non-infected at the time of viral introduction.

Memory T-cells may be infected directly by virus at a rate of $\omega_1 = k\alpha_v(v_E + v_I)$, entering the T_m^* population. The coefficient α_v represents the reduced likelihood of resting T-cell infection due to lower expression of the the CD4 surface receptor compared to active T-cells, v_E is the amount of free virus in the LP (Equation (7)), and v_I represents the amount of free virus in the GLN given by

$$v_I = N_E(T^{I*} + R^{I*}) + N_D D^{I*}. \tag{15}$$

Infected cells of the T_m^* population may also be created from de-activated infected T-helper cells (discussed below), represented by the term $\nu_T \mu_T T^{E*}$ in Equation (10). The model assumes infected, presenting DC does not pass virus to resting T-cells upon transient association in the absence of T-cell receptor (TcR) stimulation.

Upon contact with antigen-presenting dendritic cells, a resting T-cell, infected or non-infected, is stimulated to an active Th1 in either the inductive site or the effector site. T^I (Equation (11)) and T^{I*} (Equation (12)) are the respective concentrations of non-infected and infected Th1 cells in the inductive site. T^E (Equation (13)) and T^{E*} (Equation (14)) are the concentrations of non-infected and infected Th1 in the effector site. As an example, this stimulation is represented in Equation (11) by the term $0.6 p_t k\alpha_T T_m D^I$, where p_t is the number of daughter cells produced from one central memory T-cell upon stimulation and subsequent proliferation, α_T is the probability of stimulation representing the antigen specificity of the T-cell receptor, and 0.6 is the fraction of T-cells that are central memory T-cells and, therefore, in contact with dendritic cells of the inductive site, D^I. This fraction is based on a study in mice that showed 60% of CD8+ memory T-cells created in response to lymphocytic choriomeningitis virus were $CD62L+$, a marker for central memory versus effector memory T-cells [42]. Such *in vivo* data was not found for CD4+ T-cells specifically. Similarly, the term $0.4 p_T k\alpha_T T_m D^E$ in Equation (13) represents T-cell stimulation in the effector site, where the number of daughter cells produced from one stimulated effector memory T-cell, p_T, differs from that of central memory T-cells such that $p_T < p_t$ [21]. Both p_T and p_t are functions of nTreg concentrations representing the fact that activated nTreg inhibit conventional T-cell proliferation [51], and they are given by

$$p_t = \frac{p_{t0}}{1 + m(R^I + R^{I*})} \quad \text{and} \quad p_T = \frac{p_{T0}}{1 + m(R^E + R^{E*})}. \tag{16}$$

Here m is a positive constant used to determine the effect of nTreg on Th1 proliferation, p_{t0} and p_{T0} denote the number of daughter cells produced by one proliferating T-cell (without inhibition) in the GLN and LP, respectively.

The term $\varepsilon_t(D^I + \delta D^{I*})D^I$ in Equation (11) represents additional naive T-cells that may be recruited by factors secreted by presenting dendritic cells, where the parameter ε_t is the number of T-cells recruited by one active dendritic cell. The parameter δ represents the extent to which HIV infection impairs secretion of recruitment factors by dendritic cells as well as their ability to stimulate T-cells to inflammatory phenotype. These cells may then be stimulated with a probability of α_t, generally less than the probability α_T of memory T-cell stimulation [29]. The rates at which resting T-cells infiltrate the tissue from the blood is assumed to be independent of the current tissue concentration. De-activation of active T-cells occurs at a rate of μ_T. Upon de-activation a fraction, ν_T, of T-cells re-enter the memory T-cell population and the remainder are removed through apoptosis.

T-cells in either tissue site may enter the infected compartments, T^{E*} or T^{I*}, through the following pathways: i) Direct infection by virus. This occurs at a rate of $\omega_2 = kv_e$ and $\omega_3 = kv_I$, the rate of contact with free virus in the effector and inductive sites, respectively. As described, v_E and v_I are functional parameters representing the amount of free virus in the different tissue sites. ii) Stimulation of naive T-cells and cells of the T_m population by virus-harboring individuals of the D^{I*} and D^{E*} populations represented by the first and second terms of Equation (12) and the second term in Equation (14). iii) Re-stimulation of latently infected memory T-cells of the T_m^* (Equation (10)) population represented by the fourth term in Equation (12) and Equation (14). As mentioned above, the coefficient δ is included in the stimulation terms as the study conducted in [22] specifically demonstrated that HIV infected dendritic cells isolated from chronically infected patients have a reduced ability to stimulate T-cells to an inflammatory phenotype *in vitro*. The model does not include passage of virus directly from a presenting, infected DC to an active Th1 or nTreg. Exclusion of this mode of infection assumes that a presenting DC would not associate with a T-cell that is already stimulated and in association with another DC.

2.3 CD4+ Natural T-regulatory Cells

The scheme for the dynamics of CD4+ nTreg cells is depicted in Figure 4. The correspond-
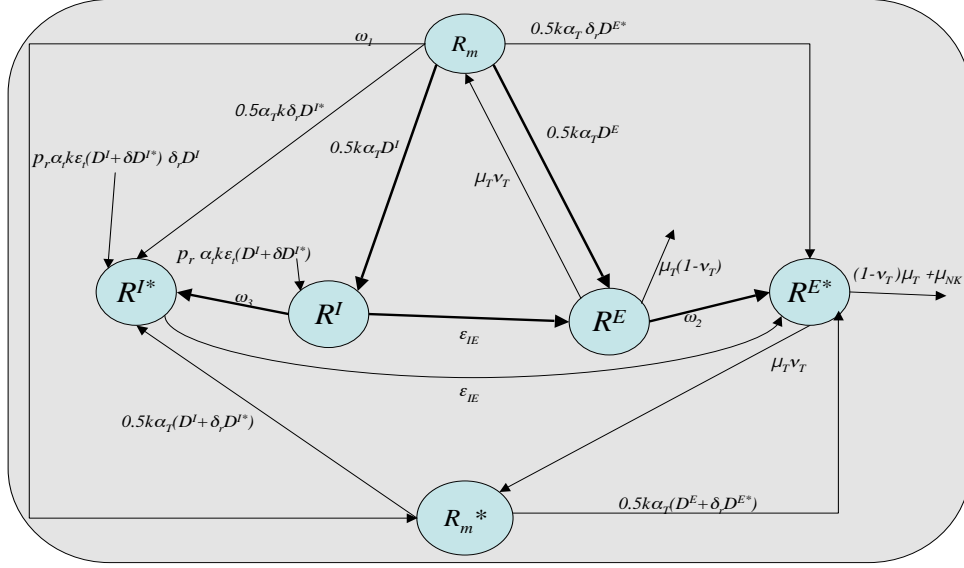
Figure 4: Scheme for dynamics of CD4+ nTreg cell populations represented.

ing compartment model for describing its dynamics is given by

$$\dot{R}_m = \nu_T \mu_T R^E - (k\alpha_T(D^E + D^I + \delta_r(D^{E*} + D^{I*})) + \omega_1)R_m, \tag{17}$$

$$\dot{R}_m^* = \omega_1 R_m + \nu_T \mu_T R^{E*} - k\alpha_T(D^E + D^I + \delta_r(D^{E*} + D^{I*}))R_m^*, \tag{18}$$

$$\dot{R}^I = p_r k\alpha_t(\varepsilon_t(D^I + \delta D^{I*}))D^I + 0.5k\alpha_T R_m D^I - (\varepsilon_{IE} + \omega_3)R^I, \tag{19}$$

$$\dot{R}^{I*} = p_r k\alpha_t(\varepsilon_t(D^I + \delta D^{I*}))(\delta_r D^{I*}) + \omega_3 R^I$$
$$+ 0.5k\alpha_T(D^I + \delta_r D^{I*})R_m^* - \varepsilon_{IE}R^{I*}, \tag{20}$$

$$\dot{R}^E = \varepsilon_{IE}R^I + 0.5k\alpha_T R_m D^E - (\mu_T + \omega_2)R^E, \tag{21}$$

$$\dot{R}^{E*} = \varepsilon_{IE}R^{I*} + 0.5k\alpha_T(D^E + \delta_r D^{E*})R_m^*$$
$$+ 0.5k\alpha_T \delta_r D^{E*}R_m + \omega_2 R^E - (\mu_T + \mu_{NK})R^{E*}. \tag{22}$$

The life cycle of non-infected and infected CD4+ nTreg is similar to that of T-helper cells, described above, where R_m represents the non-infected memory CD4+ nTreg population (Equation (17)), R^I represents non-infected active CD4+ nTreg in the inductive site

(Equation (19)), and R^E represents non-infected active CD4+ nTreg in the effector site (Equation (21)). Memory CD4+ nTreg (R_m) are assumed equally distributed into effector memory cells and central memory cells in the LP and GLN respectively. This is reflected in the terms $0.5k\alpha_T R_m D^I$ in Equation (19) and $0.5k\alpha_T R_m D^E$ in Equation (21). The model assumes the same μ_T and ν_T for CD4+ nTreg as for T-helper cells. However, there is evidence that CD4+ nTreg may not undergo activation-induced cell death (apoptosis) as readily in cell culture [52]. Stimulation of each implied naive CD4+ nTreg results in p_r daughter cells that may differ from that of conventional T-cells, p_t, and memory CD4+ nTreg do not proliferate upon re-stimulation by DC.

The model seeks to explore the net effect when CD4+ nTreg stimulation is coupled with the inflammatory response to HIV presence. As such, the same number of CD4+ nTreg is recruited by virus-presenting DC as T-helper cells (ε_t) and resting CD4+ nTreg are stimulated with the same probability (α_T). Though the mucosal site is believed to include a constant level of active CD4+ nTreg stimulated by self antigen, this baseline population is not included in the model. Including this constitutively active CD4+ nTreg population, independent of HIV presence, is assumed to have little impact on model predictions according to lack of sensitivity of model variables to initial values for $R^E(0)$ and $R^I(0)$.

Infected DC that are less able to stimulate T-helper cells to an inflammatory phenotype, discussed above, may still be able to efficiently stimulate resting CD4+ nTreg cells. This is due to the fact that impairment of DC activity includes lower levels of CD80 expression and secretion IL-10, all of which have been implicated in inducing Treg phenotypes in resting T-cells [51]. A value of 1 assigned to the parameter δ_r allows infected DC to retain the full capacity to stimulate CD4+ nTreg cells even when the ability to induce a Th1 phenotype is reduced, i.e., $\delta < 1$.

3   Model Calibration and Analysis

The model contains 17 variables and 25 constant parameters. Equations (1)-(5), (9)-(14) and (17)-(22) were first written as a vector system

$$\dot{\bar{x}} = g(\bar{x}; \bar{\theta}), \quad \bar{x}(0) = \bar{x}_0,$$

where $\bar{x} = (D_i, D^I, D^{I*}, D^E, D^{E*}, T_m, T_m^*, T^I, T^{I*}, T^E, T^{E*}, R_m, R_m^*, R^I, R^{I*}, R^E, R^{E*})^T$, $\bar{\theta}$ is the vector for model parameters, and $\bar{x}_0$ is the set of initial conditions. We followed standard practice (e.g., see [4, 9]) and solutions were determined for a log-transformed system as this resolves the problem of states becoming unrealistically negative due to computer round-off errors. As values of the model parameters are in dramatically different scales, from 10^{-8} to 10^8, all of the parameter values are also transformed to the log scale.

Therefore, let $x_i = \log_{10}(\bar{x}_i)$ and $x_{0i} = \log_{10}(\bar{x}_{0i})$, where $i = 1, 2, 3, ..., 17$ and $\theta_i = \log_{10}(\bar{\theta}_i)$ for $i = 1, 2, 3, ..., 25$. Then we have

$$\dot{x} = f(x; \theta), \quad x(0) = x_0, \tag{23}$$

where $f = (f_1, f_2, ..., f_{17})^T$ is given by

$$f_i(x; \theta) = \frac{10^{-x_i}}{\ln(10)} g_i(\bar{x}, \bar{\theta}), \quad i = 1, 2, ..., 17.$$

3.1   Simulation Setup

Simulations were carried out by solving the log transformed versions of Equations (1)-(5), (9)-(14) and (17)-(22) in MATLAB with ODE solver 23 (ode23tb) over a time course of 60 units, corresponding to two weeks where one time unit is 6 hours. Parameter values used are listed in the third column of Table 7 of Appendix A. The values of these parameters were either derived from published experimental studies (a process that is described in more detail in the Appendix A) or arbitrarily assigned if there is no studies related to them. For those parameters whose values can be found or derived from the literature, the reference numbers were given after their values, and the species from which *in vivo* these measurements were taken or cells were isolated for measurements *in vitro* were indicated after the reference numbers with "M" for "mouse", "H" for "human", and "NS" for "not specified". Ideally, one would have parameter values based exclusively on *in vivo*, human data. However, as previously mentioned such data is sparse in the current literature. Therefore, though our primary interest is to model the dynamics of early HIV infection in humans, we found it necessary to use the values obtained from other mammalian species, and assume that humans and other mammalian species have the similar parameter values.

Simulations begin at the time of viral budding from the small first generation of infected host cells, approximately on day 3 post-infection, the time at which SIV DNA is detected in cells of infected rhesus macaque tissue [47, 24]. Initial cell concentrations are given in Table 6 and are chosen so that only resting immune cells are present at the time of infection assuming no significant immune activation at the time of infection in an otherwise healthy individual. The initial infected cell population is seeded in the LP and is evenly divided among conventional T-helper cells, dendritic cells, and CD4+ nTreg cells as the demographics of this first generation of hosts is not known. The initial infected cell concentrations are based on experimental measurements taken from rhesus macaques infected with SIV reported in [47] in which the authors quantified vRNA levels, a marker of free virus and productively infected cells, in vaginal mucosa and lymph nodes during the first days of infection. The infected cell population was weighted in the LP compartment based on the observations in the same study that during the first 3 days of infection this is the

18

site where most productively infected cells were detected with only a very small number in the vaginal lymphoid tissues.

3.2 Sensitivity Analysis

In practice, one may often be in the situation of estimating a large number of unknown parameters with a limited set of data (which is true for our case). To mitigate some of this difficulty, sensitivity analysis has been widely used in inverse problem investigations (e.g., [8, 10, 11, 12, 13, 15] and the references therein) to identify the model parameters and/or initial conditions to which the model outputs (observations) are most sensitive and for which one can readily construct confidence intervals when they are estimated (i.e., which are the most reliably estimated values). Moreover, recently developed methods [8] for parameter subset selection have proven quite useful in systematically identifying the parameters or subsets of parameters that one can reasonably expect to estimate with a given data set. Some parts of this recently developed methodology [12, 13] also include new methods to assist in *design of experiments* in the context of investigations such as those initiated here.

To compute the sensitivities of model outputs to the model parameters and initial conditions, one need to know the sensitivity of each model state to each parameter and initial condition. Sensitivities $\dfrac{\partial x_i}{\partial \theta_j}$ of each variable x_i to each parameter θ_j can be determined by (see, for example, [10] and the references therein)

$$\frac{d}{dt}\frac{\partial x_i}{\partial \theta_j} = \sum_{l=1}^{17} \frac{\partial f_i}{\partial x_l}\frac{\partial x_l}{\partial \theta_j} + \frac{\partial f_i}{\partial \theta_j}, \quad \frac{\partial x_i}{\partial \theta_j}(0) = 0, \quad i = 1, 2, ..., 17, \quad j = 1, 2, ..., 25. \tag{24}$$

Corresponding sensitivities of each variable, x_i, to each initial condition, x_{0j} (the jth component of x_0) can be determined by

$$\frac{d}{dt}\frac{\partial x_i}{\partial x_{0j}} = \sum_{l=1}^{17} \frac{\partial f_i}{\partial x_l}\frac{\partial x_l}{\partial x_{0j}}, \quad \frac{\partial x_i}{\partial x_{0j}}(0) = \delta_{ij}, \tag{25}$$

where $\delta_{ij} = \begin{cases} 1, & \text{if } i = j \\ 0, & \text{if } i \neq j \end{cases}$, $i = 1, 2, ..., 17$ and $j = 1, 2, ..., 17$. These sensitivities were calculated by solving Equations (23), (24), and (25) simultaneously in MATLAB with ODE solver 15s using initial concentrations and parameter values listed in Table 6 and the third column of Table 7, respectively. Results of the sensitivity analysis informed which parameters were estimated as well as the confidence intervals for these estimated parameters are described in the section below.

19

3.3 Parameter Estimation

Proper calibration and validation of this model for the use of predicting HIV dynamics requires longitudinal data of infected and non-infected immune cells in vaginal and gut tissue during acute infection. As mentioned earlier such data was not found in the literature. Rather, we use aggregate vRNA levels obtained by euthanizing monkeys infected with SIV on different days post-infection [47]. The generally accepted biological model for acute viremia assumes a continual time course on which these averaged measurements lie and is described in Haase [24]. Following this biological model, we fit a general curve through three data points for vRNA concentration in the LP and GLN at days 3, 7, 15 and days 3, 10, 15 post-infection, respectively. These data points are estimated averages of multiple, divergent samples taken from different monkeys and are reported in Miller et al. [47]. The vRNA concentrations reported in [47] were in units of (μg vRNA)/ (1μg total tissue RNA). To map these concentrations to model variables, we make the approximation that (1μg vRNA) / (1μg total tissue RNA) = (1 infected cell or virion)/ (1μg tissue), and use the conversion that $1\mu g$ of tissue $= 10^{-6}$mL assuming that $1g$ of tissue = 1mL [23].

The mathematical model was calibrated using two synthetic data sets composed of points on these curves, which conform to the trajectory proposed by Haase[24] and Miller et al. [47] for total amount of free virus and productively infected cells in the vaginal LP and GLN during the acute phase of infection. Synthetic data set 1 (depicted by '+' in Figure 5) contains values of vRNA in the vaginal LP at various time points over a 2 week period, and synthetic data set 2 (depicted by diamonds in Figure 5) contains values of vRNA in the GLN over the same time period. As shown in Figure 5, the trajectory specifies an exponential growth from an initial value of approximately $10^4 mL^{-1}$ on day 3 post-infection to a peak value of $10^9 mL^{-1}$ on day 8 post-infection in the LP and a similar rise to $10^{10} mL^{-1}$ in the GLN.

Note that the synthetic data include the total amount of free virus and productively infected cells (i.e., total amount of vRNA) in the LP and the total amount of free virus and productively infected cells in the GLN. For system (1)-(5), (9)-(14) and (17)-(22), the total amount of free virus and productively infected cells in the LP is given by

$$\bar{z}_1(t) = N_E(T^{E*}(t) + R^{E*}(t)) + N_D D^{E*}(t) + T^{E*}(t) + R^{E*}(t) + D^{E*}(t), \qquad (26)$$

and the total amount of free virus and productively infected cells in the GLN is

$$\bar{z}_2(t) = N_E(T^{I*}(t) + R^{I*}(t)) + N_D D^{I*}(t) + T^{I*}(t) + R^{I*}(t) + D^{I*}(t). \qquad (27)$$

Specifically, the sum of the first two terms in (26) an (27) are used to account for the total amount of free virus in the LP and GLN, respectively, and the sum of the last three terms are the total amount of productively infected cells in the LP and GLN, respectively. Note

that all the equations in the system (1)-(5), (9)-(14) and (17)-(22) are coupled together. Hence, the values of $\bar{z}_1$ and $\bar{z}_2$ depend on all the model parameters and initial conditions, either strongly or weakly.

Let $z_i = \log_{10}(\bar{z}_i)$, where $i = 1, 2$. Then the norm of sensitivities of each z_i to each parameter, θ_j, and each initial condition x_{0j} was calculated with

$$\hat{z}_i(\theta_j) = \sqrt{\sum_{l=1}^{60} \left[\frac{\partial z_i}{\partial \theta_j}(t_l) \right]^2}, \quad j = 1, 2, ..., 25,$$

and

$$\hat{z}_i(x_{0j}) = \sqrt{\sum_{l=1}^{60} \left[\frac{\partial z_i}{\partial x_{0j}}(t_l) \right]^2}, \quad j = 1, 2, ..., 17,$$

respectively, where $i = 1, 2$. Based on the values of $\hat{z}_1$ and $\hat{z}_2$, the 11 parameters to which z_1 and z_2 are most sensitive are k, N_E, α_T, c_{NK}, p_{T0}, α_m, δ, ε_{IE}, ε_{EI}, λ and k_T (in the descending order), and these parameters will be estimated during the first iteration of parameter estimation process (see details below).

Let $t_i^1, i = 1, 2, \ldots, n_1$ and $t_i^2, i = 1, 2, \ldots, n_2$ denote the measurement time points for synthetic data sets 1 and 2, respectively, $\bar{y}_i^1$ be the observed total amount of vRNA in LP at time point t_i^1, $i = 1, 2, \ldots, n_1$, and $\bar{y}_i^2$ be the observed total amount of vRNA in GLN at time point t_i^2, $i = 1, 2, \ldots, n_2$. We define $y_i^1 = \log_{10}(\bar{y}_i^1)$, $i = 1, 2, \ldots, n_1$, and $y_i^2 = \log_{10}(\bar{y}_i^2)$, $i = 1, 2, \ldots, n_2$. The statistical model is assumed to have the form

$$\begin{aligned} Y_i^1 &= z_1(t_i^1; q) + \epsilon_i^1, \quad i = 1, 2, \ldots, n_1, \\ Y_i^2 &= z_2(t_i^2; q) + \epsilon_i^2, \quad i = 1, 2, \ldots, n_2, \end{aligned} \tag{28}$$

where $q \in \mathbb{R}^\kappa$ denotes vector of the estimated parameters (κ is a positive integer, and denotes the number of estimated parameters), and the observation errors $\epsilon_i^1, i = 1, 2, \ldots, n_1$ and $\epsilon_i^2, i = 1, 2, \ldots, n_2$ are independent and identically distributed with zero mean and variance σ_0^2 (log transforms are commonly used in the literature to provide nearly uniform variance, for example, they have been used in [4, 9] for other HIV models). With this assumption, q can be estimated by using an ordinary least squares (OLS) technique

$$\hat{q} = \arg\min_{q \in \mathcal{Q}} \left[\sum_{i=1}^{n_1} \left| z_1(t_i^1; q) - y_i^1 \right|^2 + \sum_{i=1}^{n_2} \left| z_2(t_i^2; q) - y_i^2 \right|^2 \right], \tag{29}$$

where $\mathcal{Q}$ is some compact set in $\mathbb{R}^k$. Then the bias adjusted estimate for σ_0^2 (e.g., see [10]) is given by

$$\hat{\sigma}^2 = \frac{1}{n_1 + n_2 - \kappa} \left[\sum_{i=1}^{n_1} \left(z_1(t_i^1; \hat{q}) - y_i^1 \right)^2 + \sum_{i=1}^{n_2} \left(z_2(t_i^2; \hat{q}) - y_i^2 \right)^2 \right].$$

21

As expected, we have a large parameter set with little experimental data. Hence, to have initial estimates, the parameter estimation was implemented in an iterative process similar to that used in [4, 9] (this approach was also required for those modeling efforts even though substantially more longitudinal data was available to support those modeling efforts). We first estimate those 11 parameters deemed most influential (by sensitivity analysis) on z_1 and z_2 with all the other parameters remained with the values assigned in the third column of Table 7. We then fix 3 of these 11 parameters at their OLS estimates and re-estimate the remaining 8 parameters, and the OLS estimates for these 3 fixed parameters (δ, ε_{IE} and ε_{EI}) are illustrated in the first three rows of Table 2. Lastly, we fix 3 of these 8 parameters

Table 2: The OLS estimates for those estimated parameters.

Parameter	Symbol	OLS Estimate
Coefficient determining effect of infection on DC functions	δ	0.74
Rate of cell migration from GLN to the LP	ε_{IE}	0.155/6hr
Rate of cell migration from LP to the GLN	ε_{EI}	0.11/6hr
Number of daughter cells produced by one T-cell in the LP, uninhibited	p_{T0}	299
Probability of infection of DC	α_m	0.04
The rate at which μ_{NK} rises to its maximum	λ	$1.31 \cdot 10^{-8}$ mL/cells
General contact rate	k	$1.08 \cdot 10^{-8}$ mL/(cells·$6hr$)
Number of free virus produced by one T-cell	N_E	300
Probability of memory T-cell stimulated by DC	α_T	10^{-3}
The maximum value of μ_{NK}	c_{NK}	51.2/6hr
Contact rate between active DC and CD4+ nTreg	k_T	$2.38 \cdot 10^{-5}$ mL/(cells·$6hr$)

at their new OLS estimates and re-estimate the remaining 5 parameters, and the OLS estimates for these 3 newly fixed parameters (p_{T0}, α_m and λ) and these 5 re-estimated ones (k, N_E, α_T, c_{NK} and k_T) are given respectively in the middle three rows of Table 2 and the last five rows of this table. The choice of the parameters to be fixed during the last two iterations is based on the combination of sensitivity analysis, the confidence we had in the estimated value as well as the knowledge we had on these parameters. The values for these 11 parameters illustrated in Table 2 will be used in the subsequent simulations where all the other parameters remain with the values assigned in the third column of Table 7.

Even though the data we have are not from experiments, we provide a way (which can be employed once the experimental observations are available) to quantify the uncertainty in our parameter estimation. There are two methods that have been widely used in the literature to quantify uncertainty in parameter estimates, one is bootstrapping and the other is asymptotic theory. These two methods have been investigated and computationally compared in [14] for problems with different form and level of noise. It was found that asymptotic theory is always faster computationally than bootstrapping, and there is no clear advantage in using the bootstrapping and asymptotic theory when the constant variance data using OLS is assumed. Based on these findings, we will use asymptotic theory in this paper to quantify the uncertainty in parameter estimation.

Let $\mathcal{Z}(q) = (z_1(t_1^1; q), z_1(t_2^1; q), \ldots, z_1(t_{n_1}^1; q), z_2(t_1^2; q), z_2(t_2^2; q), \ldots, z_2(t_{n_2}^2; q))^T$. Then the sensitivity matrix $\chi(q)$ is $(n_1 + n_2) \times \kappa$ matrix with its $(i, j)th$ element being defined by $\dfrac{\partial \mathcal{Z}_i(q)}{\partial q_j}$, $i = 1, 2, \ldots, n_1 + n_2$ and $j = 1, 2, \ldots, \kappa$, where $\mathcal{Z}_i$ is the ith element of $\mathcal{Z}$, and q_j is the jth element of q. Then by the asymptotic theory (e.g., see [10, 50] and the references therein), we know that the OLS estimator $\widehat{Q}$ is asymptotically normally distributed

$$\widehat{Q} \sim \mathcal{N}(q_0, \Sigma_0). \tag{30}$$

Here q_0 denotes the true value of the estimated parameter vector q, and Σ_0 is given by

$$\Sigma_0 = \sigma_0^2 \left[(\chi(q_0))^T \chi(q_0) \right]^{-1}.$$

Since the true value q_0 and the variance σ_0^2 are unknown, we follow the standard statistical practice by using the OLS estimates $\hat{q}$ and $\hat{\sigma}^2$ for q_0 and σ_0^2, respectively. Hence, the asymptotic properties of the least squares estimator $\widehat{Q}$ can be approximated by

$$\widehat{Q} \sim \mathcal{N}\left(\hat{q}, \widehat{\Sigma}\right), \tag{31}$$

where

$$\widehat{\Sigma} = \hat{\sigma}^2 \left[(\chi(\hat{q}))^T \chi(\hat{q}) \right]^{-1}.$$

Then the standard error $\text{Std}(\hat{Q}_j)$ for the jth element of $\hat{Q}$ is calculated by $\text{Std}(\hat{Q}_j) \approx \sqrt{\widehat{\Sigma}_{jj}}$, where $\widehat{\Sigma}_{jj}$ is the (j, j)th entry of covariance matrix $\widehat{\Sigma}$. Hence, the endpoints of the confidence intervals for $\widehat{Q}_j$ (the jth element of $\widehat{Q}$), $j = 1, 2, \ldots, \kappa$, are given by

$$\hat{q}_j \pm t_{1-\alpha/2} \, \text{Std}(\hat{Q}_j),$$

where $t_{1-\alpha/2}$ is a distribution value that is determined from a statistical table for Student's t-distribution based on the level of significance α.

For the results we report in the following, we choose $\alpha = 0.05$, which corresponds to $t_{1-\alpha/2} = 1.96$ when the number of degrees of freedom is greater than or equal to 30 (e.g.,

see [11] and the references therein), which is true for our case ($n_1 = 31$, $n_2 = 24$ and $\kappa = 5$). Table 3 illustrates the endpoints of the 95% confidence intervals (i.e., $\alpha = 0.05$) for those 5 estimated parameters illustrated in last five rows of Table 2 (i.e., those 5 parameters that are estimated during the last iteration of parameter estimation process). From this table,

Table 3: The endpoints of the 95% confidence intervals for q.

Parameters	$\hat{q}_j \pm 1.96 \, \text{Std}(\widehat{Q}_j)$	Parameters	$\hat{q}_j \pm 1.96 \, \text{Std}(\widehat{Q}_j)$
$\log_{10}(N_E)$	2.477 ± 0.078	$\log_{10}(c_{NK})$	1.709 ± 0.025
$\log_{10}(\alpha_T)$	-3.000 ± 0.069	$\log_{10}(k)$	-7.966 ± 0.027
$\log_{10}(k_T)$	-4.623 ± 0.455		

we see that the confidence intervals for all these estimated parameters are reasonably small in comparison to their corresponding estimated values.

Figure 5 illustrates the fits to the data. From this figure, we see that we have pretty good fits to the data. Hence, by this figure and Table 3 we may infer that the goodness-to-fit is
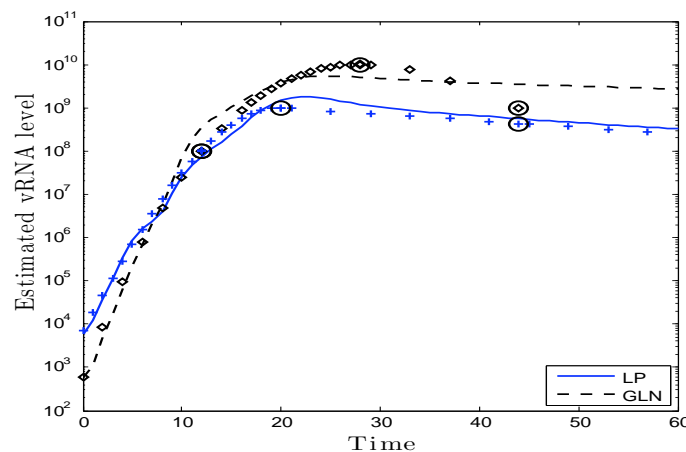

Figure 5: **vRNA levels.** Solid and dashed lines indicate vRNA levels predicted by the mathematical model in the LP and GLN, respectively. The marker '+' indicates synthetic data set 1, and diamonds represent synthetic data set 2. Circled points indicate those estimated by Haase et al. [24] directly from experimental data where vRNA values were averaged over widely varied samples reported in Miller et al [47].

reasonably well.

3.4 Partial Qualitative Validation

As we have already mentioned, sufficient experimental data is not available to fully validate our proposed model. Nonetheless, we make a first attempt to partially support and qualitatively validate this initial modeling effort with synthetic data produced from limited experimental data in the literature. The model was fit to log vRNA levels. The partial qualitative validation is carried out by comparing the underlying cell dynamics. Specifically, those for T-cells in the lymphoid tissue (Figure 6) were compared to those observed in SIV models of acute infection. In agreement with Li et al., [39] and Estes et al., [20], the
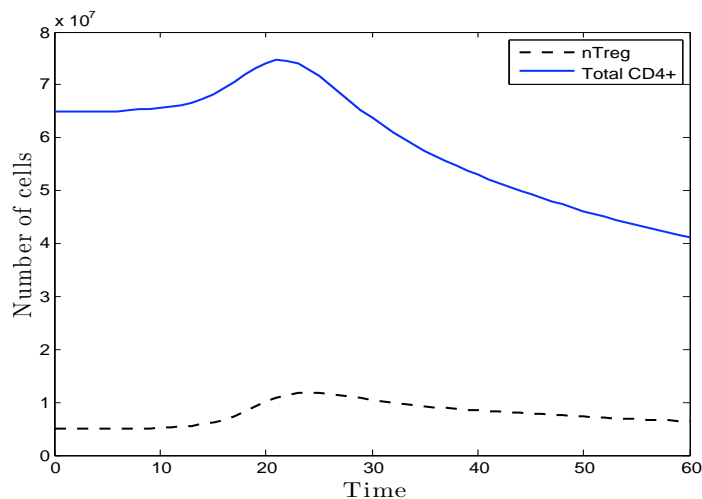

Figure 6: Simulated timecourse of total CD4+ T-cells (solid line) and CD4+ nTreg (dashed line) in lymphoid tissue following infection of first host generation.

model predicts an initial influx of CD4+ T-cells, both helper and regulatory, to the site of infection. This influx is followed by a decrease in the total CD4+ T-cell population of the lymph node as observed by Karlsson et al., [33]. This study reported an average 20% reduction in total CD4+ T-cells in non-specific lymphoid tissue by day 14 and 50% on day 28 post-infection. Our model predicts a reduction of 22% by day 14 post-infection that continues to a 46% reduction in lymphoid T-cells by day 21 post-infection, the last time point of the simulation. In addition, non-human primate infection referenced in Hogue et al. [26] measured $1.7 \cdot 10^6 mL^{-1}$ infected cells in the lymph node on day 6 post-infection. Our model predicts $8.64 \cdot 10^5 mL^{-1}$ productively infected CD4+ T-cells in the GLN on this day.

To further test the validity of our model we observed the effect of CD4+ nTreg depletion,

represented in the model as reduced resting CD4+ nTreg at the time of infection ($R_m(0)$), on the course of viral proliferation. Though it has been observed that Treg cells from hosts infected with HIV and FIV (feline immunodeficiency virus) suppress antiviral responses during the chronic stage of infection [1, 34, 46], a recent study in FIV shows that Treg cell depletion of approximately 78% prior to infection does not significantly impact viral load or CD4+ T cell levels in tissues [45]. When simulations were carried out with reduced $R_m(0)$ values from $10^7 mL^{-1}$ to $10^5 mL^{-1}$ and then to $10^{-10} mL^{-1}$, there was no change in the time of viral peak in either tissue site and $< 8\%$ increase in peak vRNA values in the GLN and $\leq 13.5\%$ increase in peak vRNA value in the LP, in accordance with these FIV results.

4   Simulations and Results

For each experimental condition described in the following sections, four measurements were made to determine the rate and extent of viral proliferation: i) The maximum vRNA levels $\bar{z}_{1max}$ in the LP, that is, $\bar{z}_{1max} = \max_{t \in [0,60]} \bar{z}_1(t)$, where $\bar{z}_1$ is given by Equation (26); ii) the maximum vRNA levels $\bar{z}_{2max}$ in the GLN, given by $\bar{z}_{2max} = \max_{t \in [0,60]} \bar{z}_2(t)$ with $\bar{z}_2$ defined by Equation (27); iii) the time t_{peakLP} at which the vRNA level peaks in the LP, that is, $t_{peakLP} = \arg \max_{t \in [0,60]} \bar{z}_1(t)$; and iv) the time $t_{peakGLN}$ at which estimated vRNA peaks in the GLN, that is, $t_{peakGLN} = \arg \max_{t \in [0,60]} \bar{z}_2(t)$. The latter two measurements can be interpreted as the estimated "window period" between the start of simulation and the time at which peak viremia is reached in each tissue.

As we noted earlier that all the equations in the system (1)-(5), (9)-(14) and (17)-(22) are coupled together. Hence, the values of the peak vRNA levels in LP and GLN as well as the corresponding time at which their levels peak depend on all the model parameters and initial conditions, either strongly or weakly. In this section, we will compare these four values for the null model with those representing different immunological backgrounds and interventions of interest. These include the effect of early inflammatory versus regulatory response on initial viremia, the role of CD4+ nTreg on initial viral spread, as well as the impact of inflammatory mechanisms.

4.1 Effect of Early Inflammatory vs. Regulatory Response on Initial Viremia

To assess the net effect of a enhanced inflammatory or regulatory immune response, in terms of expediency and strength, to HIV production we observed the correlation between viral spread and initial concentration of active immune cells in the LP; $D^E(0)$, $T^E(0)$, and $R^E(0)$. A set of initial concentration values for each variable were sampled from 10^{-10} to 10^{10}, where 10^{-10} is the value in the null model.

Results: In Table 4 we report estimated peak vRNA levels and their corresponding time points for the null model and in the cases of elevated initial concentration of each active cell population to $10^6 mL^{-1}$, approximately the expected concentration under normal inflammatory conditions [18]. It can be seen that none of these increases of the active immune

Table 4: Effect of immunological background on initial viremia.

Condition	$\bar{z}_{1max}$ (t_{peakLP})	$\bar{z}_{2max}$ $(t_{peakGLN})$
Null Model	$1.804 \cdot 10^9 mL^{-1}$ (23)	$5.45 \cdot 10^9 mL^{-1}$ (26)
$T^E(0) = 10^6 mL^{-1}$	$1.803 \cdot 10^9 mL^{-1}$ (19)	$5.45 \cdot 10^9 mL^{-1}$ (21)
$R^E(0) = 10^6 mL^{-1}$	$1.794 \cdot 10^9 mL^{-1}$ (21)	$5.422 \cdot 10^9 mL^{-1}$ (24)
$D^E(0) = 10^6 mL^{-1}$	$1.799 \cdot 10^9 mL^{-1}$ (23)	$5.45 \cdot 10^9 mL^{-1}$ (25)

cell populations has a significant impact on peak vRNA levels in either tissue with $\leq 0.1\%$ difference even though the initial concentration is raised by over 6 orders of magnitude. However, all have a significant impact on t_{peakLP} and $t_{peakGLN}$, representing the "window period". Specifically we show in Figure 7 that the initial level of all active immune cell populations is negatively correlated with t_{peakLP} and $t_{peakGLN}$ indicating that as their concentrations increase, virus is able to spread more rapidly. This effect is particularly pronounced for the T-cell populations, both inflammatory and regulatory, and coincides with earlier markers of the inflammatory response. Shown in Table 5 are the time points at which the peak values of functional parameters μ_{NK} and ε_m are seen as well as those at which their values initially begin to decline.

Table 5: Effect of immunological background on timing of inflammatory response.

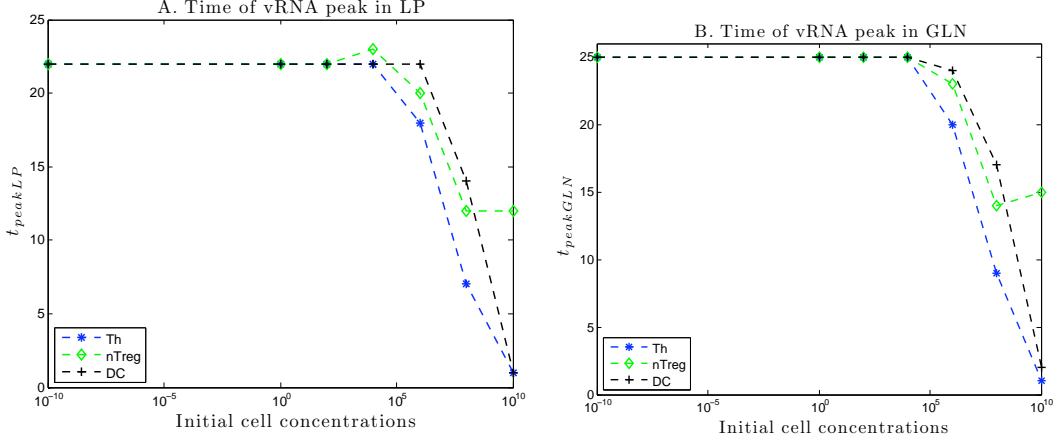| Condition	peak μ_{NK}	μ_{NK} decline	peak ε_m	ε_m decline
Null Model	28	52	22	31
$T^E(0) = 10^6 mL^{-1}$	15	47	18	27
$R^E(0) = 10^6 mL^{-1}$	18	49	22	31

Figure 7: **Effect of enhanced immune response on the rate of viral spread**: Here the predicted values of t_{peakLP} (A) and $t_{peakGLN}$ (B) are plotted against initial values of active immune cell concentrations in the LP.

Conclusions: These results have multiple implications.

An increased initial concentration of T^E can represent a recent immune response from which residual Th1 cells are still present or a very rapid inflammatory response that allows entrance of Th1 prior to viral replication in the initial host population; a possible consequence of vaccine exposure.

In 2005 the notorious STEP vaccine trial was carried out, in which high-risk participants were administered HIV protein within an adenovirus vector. This trial failed returning results indicating that vaccinated individuals were *more* likely to be infected with HIV [56]. The prevailing hypothesis for this surprising result was that the immune response elicited, by either the adenovirus vector or the HIV antigen itself, created an inflammatory environment predisposing individuals to infection upon exposure of viable HIV. The effect of enhanced $T^E(0)$ in our simulations supports this hypothesis. A vaccine-elicited inflammatory response would facilitate viral spread predisposing the host to infection if exposure occurs while it is still active. This is a probable scenario for individuals in high-risk positions such as those who received the vaccine during the trial.

The results also indicate that inducing the CD4+ nTreg response at the time of infection will likely expedite infection. The decrease in $t_{peakGLN}$ and t_{peakLP} seen with elevated $R^E(0)$ indicates that, indeed, active CD4+ nTreg has a net effect of aiding viral proliferation and dissemination, not necessarily by increasing viral production, but by expediting it. Furthermore, that this increase is not due to nTreg-mediated dampening of NK activation,

28

but rather its ability to replicate virus.

The indication is that a more rapid CD4+ nTreg response would likely not be protective against viral proliferation. This is relevant as CD4+ nTreg has been shown to promote and inhibit a successful antiviral response in different species. Specifically, SIV pathogenesis is greatly reduced in African green monkeys compared to that in rhesus macaques. It has been suggested that this may be due to the fact that the CD4+ nTreg response in African green monkeys is quicker, leading to reduced susceptible T-cell recruitment and stimulation by DC in the infection site [23, 37]. In our simulations, increasing the initial concentration of $R^E(0)$ represents an immediate CD4+ nTreg response elicited prior to viral production by the first generation of infected cells. These simulation results suggest this is not a plausible explanation for reduced viremia in green monkeys as an earlier CD4+ nTreg response has little effect on dampening the extent of viral proliferation. Rather, the sooner active CD4+ nTreg is present, even prior to the inflammatory response, the quicker virus will propagate.

4.2 The Role of CD4+ nTreg Functions in Initial Viral Spread

It was seen that active CD4+ nTreg has the effect of increasing the rate of viral dissemination. We then sought to identify the net effect of specific CD4+ nTreg functions: contact-dependent deactivation of presenting dendritic cells, governed by the parameter k_T, and inhibition of Th1 proliferation, governed by the parameter m. This was done by plotting peak vRNA levels, $\bar{z}_{1max}$ and $\bar{z}_{2max}$ (Figure 8 (A) and (B)) as well as their corresponding time points t_{peakLP} and $t_{peakGLN}$ (Figure 8 (C) and (D)) by increasing values for these parameters. Specifically, values for m, the coefficient for functional parameters p_t and p_T (defined in Equation (16)), that determines the extent to which CD4+ nTreg inhibits T-helper cell proliferation, were sampled from the range $[10^{-10}, 10^{-1}]$. Values for k_T, the rate of contact and de-activation of DC by CD4+ nTreg were taken from the range $[2.3821 \cdot 10^{-10}, 2.3821 \cdot 10^{-1}]$.

Results: Plots in Figure 8 clearly show a negative correlation between both functions and peak vRNA levels indicating that enhancement of either has a net effect of reducing viral proliferation, with k_T having a tighter correlation. In relation to the "window period" , the negative effect of k_T is also clearly demonstrated. In Figure 8 (C) and (D) it can be seen that as k_T increases from its default value, the values of t_{peakLP} and $t_{peakGLN}$ increases indicating that CD4+ nTreg-mediated DC de-activation has a net effect of prolonging the window period. Though these values are also higher than that in the null model when k_T is severely reduced, this corresponds with very high viral load that likely continues to rise uninhibited. The relationship between the window period and m appears more complex.
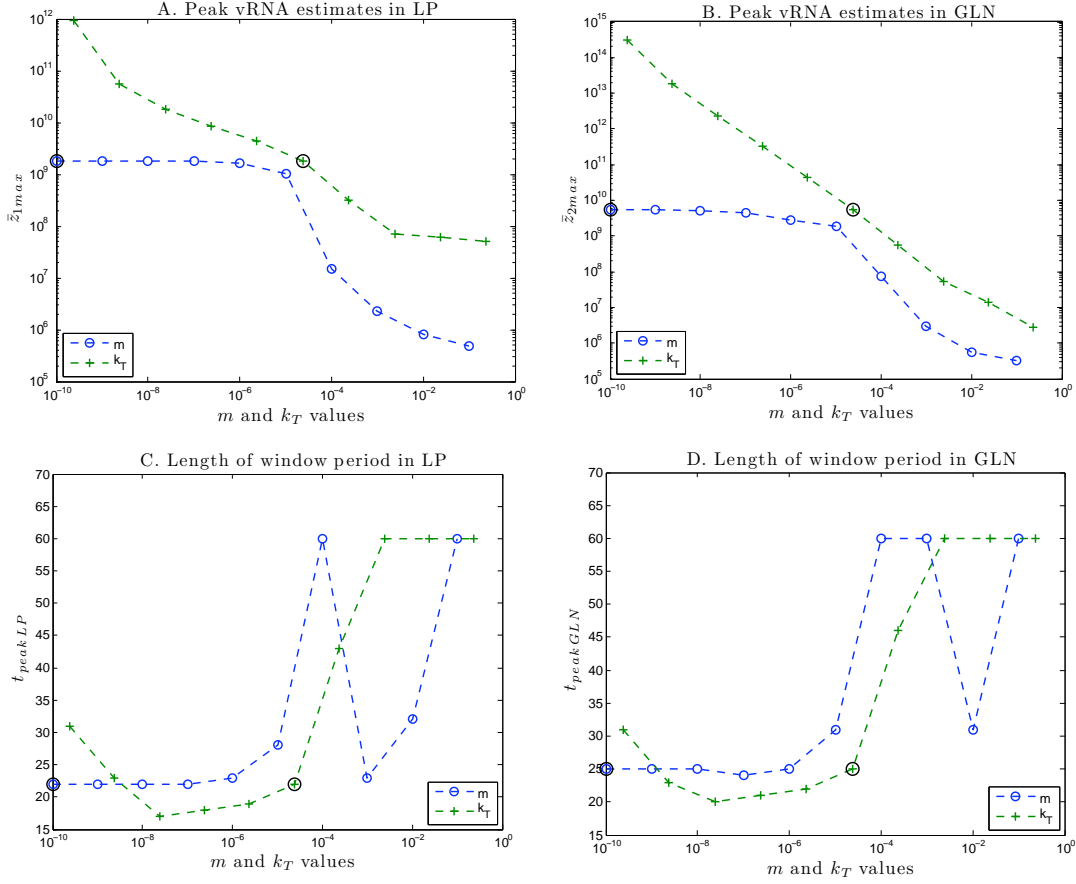
Figure 8: **Effect of CD4+ nTreg regulatory functions on viral spread**: Here the four measurements of viral spread are plotted by increasing values of the parameter m (circles) and k_T (+ sign); (A) peak level of vRNA in the LP, $\bar{z}_{1max}$, (B) peak level of vRNA reached in the GLN, $\bar{z}_{2max}$, (C) time of peak vRNA level reached in the LP, t_{peakLP}, (D) time of peak vRNA level reached in the GLN, $t_{peakGLN}$. Circled points represent parameter values in the null model.

Like k_T, as m increases from the default value the window period is increased. However, there is a range for m, 10^{-3}-10^{-2}, in which the beneficial effect is much less significant, even non-existent in the LP. This highlights the complex, non-linear relationship between m and the response of the over all system. For example, R^E is, itself, an indirect function of m as an increased m leads to decreased T^E and T^{E*}, which affects the functional parameters μ_{NK} and ε_m that directly influence the levels of R^{E*} and R^E.

We next sought to determine whether such enhancement of CD4+ nTreg functions could change its relationship to increased viral proliferation, i.e., whether enhancement of these specific functions could render the net effect of CD4+ nTreg activation to be protective. Specifically, we sought a value for these parameters at which one could clearly observe a negative correlation between peak vRNA levels, $\bar{z}_{1max}$ and $\bar{z}_{2max}$, and the initial active CD4+ nTreg concentration, $R^E(0)$, as well as a positive correlation with the window periods, t_{peakLP} and $t_{peakGLN}$. To this end, we observed the four measurements for viral proliferation against increasing values for initial active nTeg concentration, sampled from the range $[10^{-10}, 10^{10}]$ with different values for m and k_T.

Results: For all values assigned to m, from the range $[10^{-10}, 10^{-1}]$, the estimated peak vRNA levels remained positively correlated with initial active CD4+ nTreg concentration, if affected at all, and the estimated window periods remained negatively correlated (as observed from Figure 9). In the case of enhanced ability to deactivate DC, the effect is largely just as insignificant. For most values of k_T the relationship between active CD4+ nTreg and vRNA levels remains positive and that with the window period remains negative. However, it can be see in Figure 10 that for higher values of k_T, there is a specific range of initial CD4+ nTreg concentrations (about 10^2 -$10^4 mL^{-1}$) that inhibit the propagation of the first generation of free virus produced by the initial host population. In other words, viremia does rise above the concentration of approximately $10^4 mL^{-1}$. This effect on viremia in the GLN, specifically, is observed over a wider range of CD4+ nTreg concentrations than those in the LP.

Conclusions: CD4+ nTreg-mediated inhibition of DC is a useful aspect of the regulatory response that one wants to maintain offering the most promising avenue for intervention. Furthermore, with an enhanced capacity to de-activate DC, there is a range of CD4+ nTreg activation that could be protective at the time of infection.

However, manipulation of CD4+ nTreg-mediated inhibition of Th1 proliferation could have unpredictable, unintended consequences. Hence, this function is not a strong candidate for exploitation in reducing viral spread as simulations indicate that enhancing the capacity to inhibit Th1 proliferation, does not change the net effect of CD4+ nTreg activation as it continues to expedite viral proliferation due to its ability to replicate virus.

With these findings we recommend conducting carefully designed experiments to determine potential beneficial effect of promoting CD4+ nTreg-mediated DC inhibition in an *in vivo* setting of acute infection. In a similar vein, it would be interesting to experimentally observe the net effect of enhancing CD4+ nTreg-mediated inhibition of Th1 proliferation given the anti-intuitive dynamics reported here.
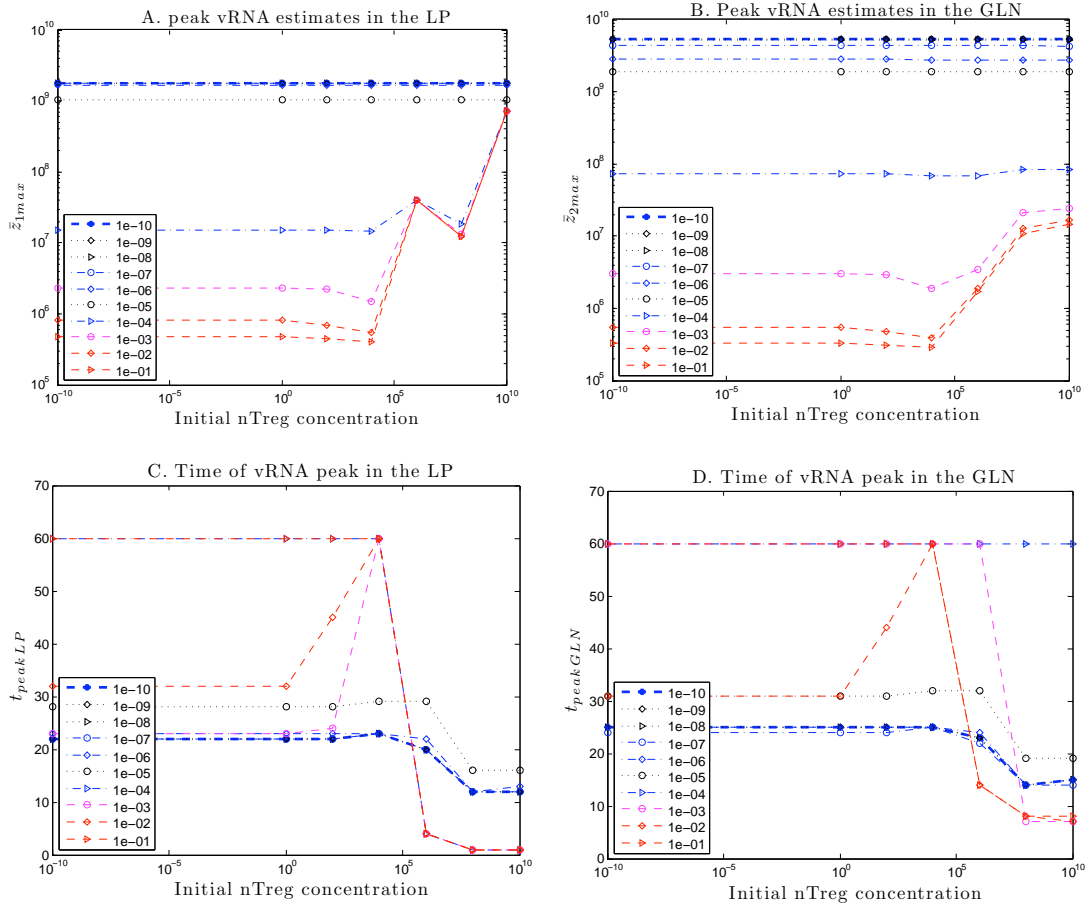
Figure 9: **Relationship between initial active nTreg concentration and viral proliferation given enhanced capacity to inhibit Th proliferation**: Here the following factors are plotted by increasing values of $R^E(0)$ given different values of m as indicated in the legend; (A) peak level of vRNA in the LP, z_{1max}, (B) peak level of vRNA reached in the GLN, z_{2max}, (C) time of peak vRNA level reached in the LP, t_{peakLP}, (D) time of peak vRNA level reached in the GLN, $t_{peakGLN}$. The thicker line represents the value of m used in the null model.

32

Figure 10: **Relationship between initial active CD4+ nTreg concentration and viral proliferation given enhanced DC-deactivation capacity**: Here the following factors are plotted by increasing values of $R^E(0)$ given different values of k_T as indicated in the legend; (A) peak level of vRNA in the LP, $\bar{z}_{1max}$, (B) peak level of vRNA reached in the GLN, $\bar{z}_{2max}$, (C) time of peak vRNA level reached in the LP, t_{peakLP}, (D) time of peak vRNA level reached in the GLN, $t_{peakGLN}$. The thicker dotted line represents the 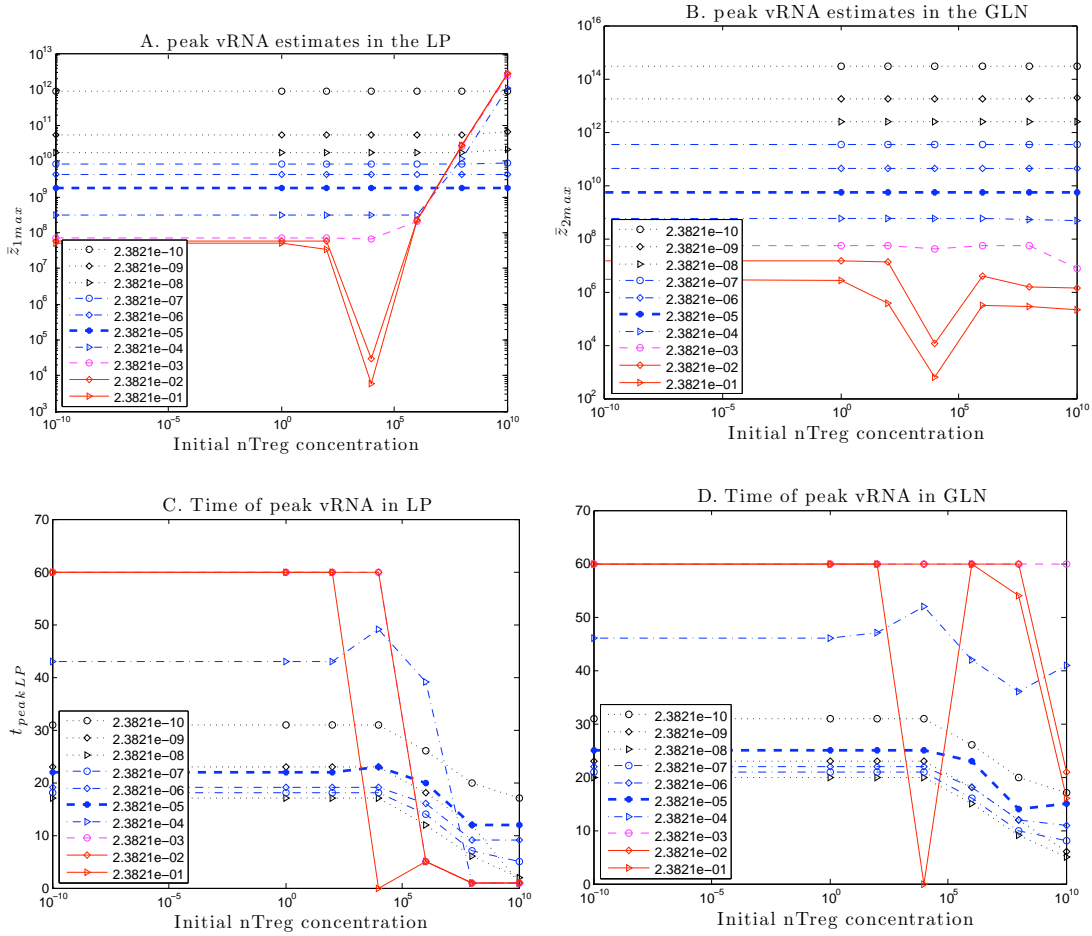value of k_T used in the null model. Solid lines indicate k_T values for which initial viremia is successfully controlled and does not rise significantly above concentration of the first generation of budded virus.

4.3 Impact of Inflammatory Mechanisms

The model includes an inflammatory response to viral production that is comprised of four main mechanisms: i) stimulation of both resting conventional T-cells and CD4+ nTreg at the rate of α_T, ii) recruitment of both resting conventional T-cells and CD4+ nTreg to the inductive site at the rate ε_t, iii) the recruitment of monocytes, immature dendritic cell precursors, at the rate ε_m (Equation (6)), mediated by the parameter c_m, and iv) removal of infected cells by NK cells at the rate μ_{NK} (Equation (8)), mediated by the parameters c_{NK}, the maximum value of the removal rate, and λ, the rate of increased removal as DC and Th1 concentrations rise. In order to clarify those mechanisms that most influenced the net positive impact of the inflammatory response on HIV spread we sought to correlate the peak vRNA levels with each the parameters governing these four mechanisms. To do this we plotted estimated peak vRNA levels in the LP ($\bar{z}_{1max}$) and in the GLN ($\bar{z}_{2max}$) by values for each parameter. Values for ε_t were sampled from the range $[10^{-10}, 1000]$, those for c_m from the range $[10^{-10}, 1000]$, those for α_T from the range $[10^{-10}, 1]$, those c_{NK} from the range $[5.12 \cdot 10^{-10}, 5.12 \cdot 10^3]$, and those for λ from the range $[10^{-10}, 10^{-1}]$.

Results: Plots in Figure 11 show that monocyte recruitment has little effect on viremic levels, with T-cell recruitment having a slightly anti-intuitive, negative effect on viral proliferation. NK activity and Th1 stimulation are the processes that play the most critical role in determining the rate of viral proliferation. Specifically, enhanced NK activity is intuitively beneficial. DC-mediated stimulation of regulatory and inflammatory T-cells, however, has a significant impact in aiding viral proliferation.

Conclusion: The positive correlation between the inflammatory response (shown in section 4.1) and expedited viremia is largely attributed to DC-mediated stimulation of T-cells, both Th1 and CD4+ nTreg. However, NK cells can be a very effective fighter against viral spread, which is significant as their activity may be elicited prior to the CD8 response through DC activation and potentially independent of CD4+ Th1 activation.

These results suggest that one would want to be specific in choosing the inflammatory function to be targeted for enhancement as an intervention strategy. T-cell recruitment by DCs may be slightly protective, but if this is coupled with Th1 stimulation, the impact can be quite negative for the host. In terms of determining inflammatory mechanisms to inhibit in order to quell viral spread, targeting DC-mediated recruitment of T-cells is not recommended as it appears to be a necessary component of the antiviral response. A better strategy would be targeted disruption of DC contact with and/or stimulation of T-cells (helper and regulatory). Indeed, simulations with reduced α_T to 10^{-10} leads to much lower viremia with no noticeable T-cell loss (results not shown).
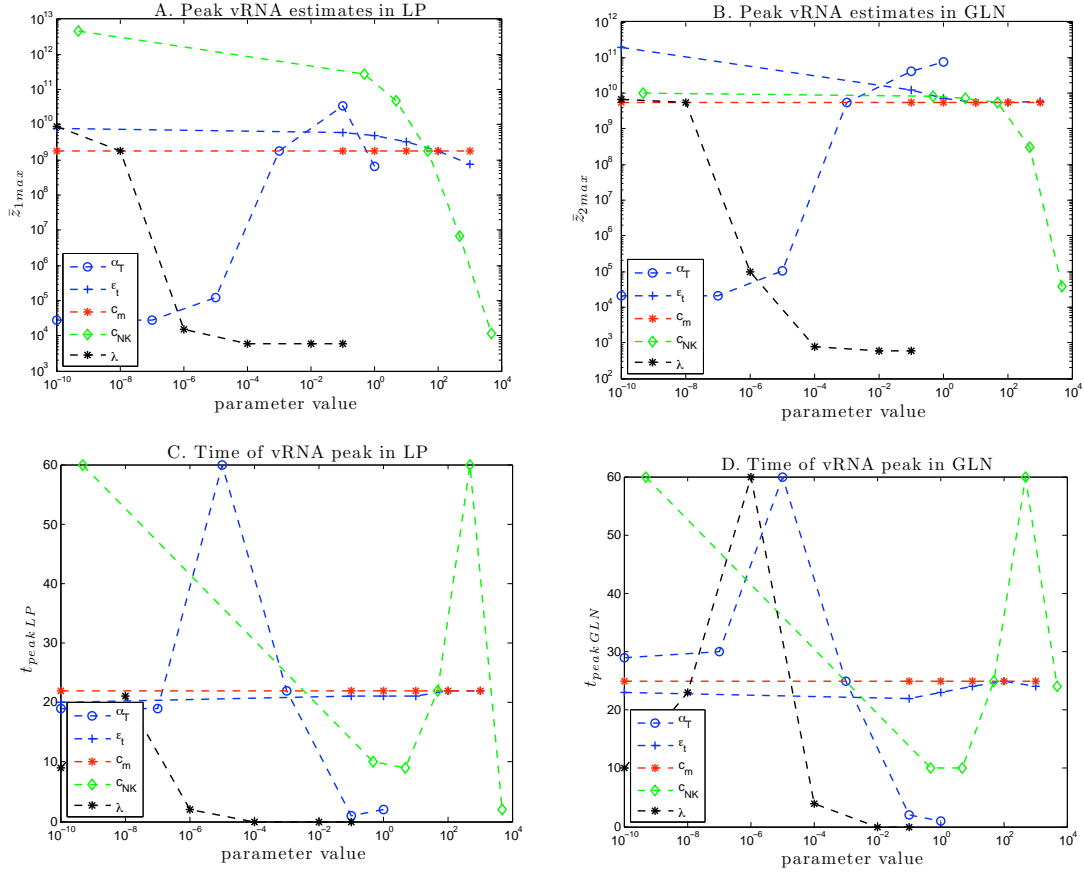
Figure 11: **Relationship between inflammatory mechanisms and acute viral spread**: Here the following factors are plotted by increasing values of c_m (red stars), ε_t (blue + sign), α_T (blue circles), c_{NK} (green diamonds), and λ (black stars). (A) peak level of vRNA in the LP, $\bar{z}_{1max}$, (B) peak level of vRNA reached in the GLN, $\bar{z}_{2max}$, (C) time of peak vRNA level reached in the LP, t_{peakLP}, (D) time of peak vRNA level reached in the GLN, $t_{peakGLN}$.

5 Discussion

Here we present a model of the HIV-specific inflammatory pathway leading to Th1 activation and the nTreg-mediated regulatory pathway that suppresses it. Simulations based on this model and its component mechanisms suggest that a global activation of either the adaptive regulatory or inflammatory response would expedite viral dissemination, over-

coming the innate antiviral response, as both lead to activation of HIV-permissive Th1 and nTreg. This result holds even over a wide range of conditions that would enhance or weaken the influence of nTreg on DC-deactivation and Th1 proliferation. Analysis of the most effective regulatory functions and harmful inflammatory mechanisms specify DC-mediated stimulation of CD4+ T-cells as the key mechanism driving viral proliferation. The indication is that once DC carries HIV to the lymph node to present to T-cells, the infection has little chance of being stopped as the virus is now in an environment with a plentitude of highly permissive hosts, has access to the blood stream, and is largely protected from NK mediated removal. Hence, any vaccine-primed responses that require this presentation upon viral challenge will occur too late and be ineffective, if not harmful. This includes a typical CD8 response which relies on the activation and proliferation of CD4+ T-cells for cytotoxic T-lymphocyte (CTL) activation. Indeed such obstacles are what have made finding an effective and protective vaccine so difficult.

This work suggests that such strategies will continually fail to control systemic spread and viremia. Rather, there should be a focus on responses that may lead to viral removal prior to interaction between a presenting infected DC and resting T-cell takes place. This may include neutralizing antibody that could, theoretically, eliminate virus prior to contact with DC by preventing transcytosis from vaginal lumen to LP or antibody-dependent cell cytotoxicity that would enhance the ability of NK cells to eliminate the initial host cell population at site of infection prior to spread.

Ideal intervention strategies would be those that enhance the innate response without a need for T-cell expansion. As an example, this could involve NK activation through selective recruitment of plasmacytoid DCs (pDCs) from the blood to the infection site as this DC subset does not play a significant role in T-cell expansion, but is effective in inducing NK response through secretion of IFN-α [5]. Though pDC has been associated with immune dysregulation, this association is seen with established viral infection in the chronic disease phase. Other strategies to enhance the effective NK response is to target viral proteins that inhibit innate immune response such as nef, which leads to downregulation of NKG2D ligands on the surface of infected cells [5].

In terms of prevention treatments that seek to exploit the innate immune response, our conclusions recommend those that could disrupt DC: T-cell interactions upon HIV entry, allowing NK activity to occur through DC stimulation alone. Such strategies may involve treatment with tolerogenic commensal bacterial strains in the vaginal lumen, inhibition of antigen presentation by DC, and targeted inhibition of DC-TcR interactions.

Knowledge of the mechanisms involved in this model is evolving. Specifically, those governing DC-mediated delivery of virus, HIV-specific NK activation, and HIV-specific activation and suppressive functions of nTreg continue to be a source of controversy in the experi-

mental HIV immunology field.

As stated in Section 2.2, it may be possible for infected DC to deliver viable virus to resting T-cells upon transient association in the absence of TcR recognition and subsequent stimulation. By not including this mechanism of contact-dependent infection of resting T-cells our model may underestimate the number of latently infected memory T-cells that may be established by a single infected DC in the early stage of infection. The possible error in size of this reservoir population presumably has little impact on the dynamics of early infection and the initial viremic spike, but will be relevant in future models that seek to encompass the chronic disease stage following the acute phase.

This model assumes that HIV-specific nTreg suppressor functions are dependent upon TcR stimulation indicated by *in vitro* observations [51] and focus on the theoretical consequences of HIV-solicited regulatory response coupled to the inflammatory response. The true mucosal system likely includes HIV-nonspecific nTreg activation pathways that may be relevant. As mentioned, the mucosal site is believed to include a constant level of active CD4+ nTreg stimulated by self antigen and commensal bacteria. This constitutively active CD4+ nTreg population could be represented as a constant in-flow into the R^E population. In addition, there may be a polyclonal nTreg population present that can be activated by TGF-β secreted from neighboring nTreg [51]. This could be represented by an influx into the R^E population proportional to the current R^E population, enhancing the effect of nTreg cell concentration on viral proliferation and NK suppression. Hence, we presume that exclusion of these mechanisms leads to simulation results that underestimate the contribution of nTreg presence to viral proliferation. The significance of such HIV-independent, polyclonal populations and circumstances governing their activation *in vivo* is largely unknown and may be incorporated into later versions of the model as more information is gathered.

Studies have indicated nTreg may have a direct cytolytic effect on NK cells. This mode of suppression was not included as it was demonstrated in a minority of nTreg in specific *in vivo* conditions of a tumor microenvironment and has not been reproducible in other situations [51, 17]. Including this mechanism would likely enhance the positive effect of nTreg activation on viral dissemination and, therefore, is not presumed to change the net effect of the regulatory response reported here. Specifically, it ultimately promotes viral proliferation.

The assumptions made here regarding mechanisms represented and excluded in the model are a subset of those currently in the literature making this model a foundation for studying various hypothesized details of each mechanism in future versions.

Given the lack of data in the current literature, this modeling effort constitutes a prelim-

inary exploration into the role of the regulatory pathway and how it may be exploited to prevent HIV proliferation. The current model is capable of addressing conceptual questions relevant to devising intervention to quell HIV spread such as those addressed here: *Should one promote the regulatory response?*, *Should one inhibit the regulatory response?* and *What specific mechanisms of inflammation would be best to suppress in a targeted manner?*

However, the model is not adequate for making quantitative predictions as this requires calibration to specific experimental data. Future work involves using this preliminary model to suggest specific experiments with which such data can be collected. A model calibrated to adequate data could then be used to make quantitative predictions of viral load and timing of systemic spread within a satisfactory level of confidence.

Acknowledgements

References

[1] E. M. Aandahl, J. Michaelsson, W. J. Moretto, F. M. Hecht, and D. F. Nixon. Human CD4+ CD25+ regulatory T cells control T-cell responses to human immunodeficiency virus and cytomegalovirus antigens. *J Virol*, 78(5):2454–9, 2004.

[2] K. Abel, D. M. Rocke, B. Chohan, L. Fritts, and C. J. Miller. Temporal and anatomic relationship between virus replication and cytokine gene expression after vaginal simian immunodeficiency virus infection. *J Virol*, 79(19):12164–72, 2005.

[3] L.J. Abu-Raddad, P. Patnaik, and J.G. Kublin. Dual infection with HIV and Malaria fuels the spread of both diseases in sub-Saharan Africa. *Science*, 314:1603–1606, 2006.

[4] B.M. Adams, H.T. Banks, M. Davidian, and E.S. Rosenberg. Model fitting and prediction with HIV treatment interruption data. *Bulletin of Mathematical Biology*, 69:563–584, 2005.

[5] M. Altfeld, L. Fadda, D. Frleta, and N. Bhardwaj. Dcs and nk cells: critical effectors in the immune response to hiv-1. *Nature Reviews Immunology*, 11(3):176–186, 2011.

[6] C. E. Andoniou, D. M. Andrews, and M. A. Degli-Esposti. Natural killer cells in viral infection: more than just killers. *Immunol Rev*, 214:239–50, 2006.

[7] M. Asano, M. Toda, N. Sakaguchi, and S. Sakaguchi. Autoimmune disease as a consequence of developmental abnormality of a T cell subpopulation. *Journal of Experimental Medicine*, 184(2):387–396, 1996.

[8] H.T. Banks, A. Cintron-Arias, and F. Kappel. Parameter selection methods in inverse problem formulation. *Proceedings Biomedical Modeling and Cardiovascular-Respiratory Control: Theory and Practice Summer School and Workshop: A Marie Curie Training Event, Springer Lecture Notes, 2011, to appear.* Center for Research in Scientific Computation Report, CRSC-TR10-03, November, 2010, NCSU, Raleigh.

[9] H.T. Banks, M. Davidian, Shuhua Hu, G.M. Kepler, and E.S. Rosenberg. Modelling HIV immune response and validation with clinical data. *J. Biological Dynamics*, 2:357–385, 2008.

[10] H.T. Banks, M. Davidian, J.R. Samuels Jr., and K. L. Sutton. An inverse problem statistical methodology summary. In Gerardo Chowell, Mac Hyman, Nick Hengartner, Luis M.A Bettencourt, and Carlos Castillo-Chavez, editors, *Statistical Estimation Approaches in Epidemiology*, pages 249–302, Berlin Heidelberg New York, 2009. Springer. Center for Research in Scientific Computation Report, CRSC-TR08-01, January, 2008, NCSU, Raleigh.

[11] H.T. Banks and J.L. Davis. Quantifying uncertainty in the estimation of probability distributions. *Math. Biosci. Eng.*, 5:647–667, 2008. Center for Research in Scientific Computation Report, CRSC-TR07-21, December, 2007, NCSU, Raleigh.

[12] H.T. Banks, Sava Dediu, Stacey L. Ernstberger, and Franz Kappel. Generalized sensitivities and optimal experimental design. *J. Inverse and Ill-posed Problems*, 18:25–83, 2010. Center for Research in Scientific Computation Report, CRSC-TR08-12, (Revised) November, 2009, NCSU, Raleigh.

[13] H.T. Banks, K.J. Holm, and F. Kappel. Comparison of optimal design methods in inverse problems. *Inverse Problems*, 27:075002, 2011. Center for Research in Scientific Computation Report, CRSC-TR10-11, July, 2010, NCSU, Raleigh.

[14] H.T. Banks, K.J. Holm, and D. Robbins. Standard error computations for uncertainty quantification in inverse problems: asymptotic theory vs. bootstrapping. *Mathematical and Computer Modelling*, 52:1610–1625, 2009. Center for Research in Scientific Computation Report, CRSC-TR09-13, Revised, May, 2010, NCSU, Raleigh.

[15] H.T. Banks and H.T. Tran. *Mathematical and Experimental Modeling of Physical and Biological Processes.* CRC Press, Boca Raton, FL, 2009.

[16] R.J. De Boer and A.S. Perelson. Target cell limited and immune control models of HIV infection: a comparison. *J. Theor. Biol.*, 190:201–214, 1998.

[17] X. F. Cao, S. F. Cai, T. A. Fehniger, J. L. Song, L. I. Collins, D. R. Piwnica-Worms, and T. J. Ley. Granzyme b and perforin are important for regulatory t cell-mediated suppression of tumor clearance. *Immunity*, 27(4):635–646, 2007.

[18] D. M. Catron, A. A. Itano, K. A. Pape, D. L. Mueller, and M. K. Jenkins. Visualizing the first 50 hr of the primary immune response to a soluble antigen. *Immunity*, 21(3):341–347, 2004.

[19] D. S. Dimitrov, R. L. Willey, H. Sato, L. J. Chang, R. Blumenthal, and M. A. Martin. Quantitation of human immunodeficiency virus type 1 infection kinetics. *J Virol*, 67(4):2182–90, 1993.

[20] J. D. Estes, Q. Li, M. R. Reynolds, S. Wietgrefe, L. Duan, T. Schacker, L. J. Picker, D. I. Watkins, J. D. Lifson, C. Reilly, J. Carlis, and A. T. Haase. Premature induction of an immunosuppressive regulatory T cell response during acute simian immunodeficiency virus infection. *J Infect Dis*, 193(5):703–12, 2006.

[21] J. Geginat, A. Lanzavecchia, and F. Sallusto. Proliferation and differentiation potential of human CD8+ memory T-cell subsets in response to antigen or homeostatic cytokines. *Blood*, 101(11):4260–6, 2003.

[22] A. Granelli-Piperno, A. Golebiowska, C. Trumpfheller, F. P. Siegal, and R. M. Steinman. HIV-1-infected monocyte-derived dendritic cells do not undergo maturation but can elicit IL-10 production and T cell regulation. *Proceedings of the National Academy of Sciences of the United States of America*, 101(20):7669–7674, 2004.

[23] A. T. Haase. Population biology of HIV-1 infection: Viral and CD4(+) T cell demographics and dynamics in lymphatic tissues. *Annual Review of Immunology*, 17:625–656, 1999.

[24] A. T. Haase. Perils at mucosal front lines for HIV and SIV and their hosts. *Nat Rev Immunol*, 5(10):783–92, 2005.

[25] A. T. Haase, K. Henry, M. Zupancic, G. Sedgewick, R. A. Faust, H. Melroe, W. Cavert, K. Gebhard, K. Staskus, Z. Q. Zhang, P. J. Dailey, Jr. Balfour, H. H., A. Erice, and A. S. Perelson. Quantitative image analysis of HIV-1 infection in lymphoid tissue. *Science*, 274(5289):985–9, 1996.

[26] I. B. Hogue, S. H. Bajaria, B. A. Fallert, S. Qin, T. A. Reinhart, and D. E. Kirschner. The dual role of dendritic cells in the immune response to human immunodeficiency virus type 1 infection. *J Gen Virol*, 89(Pt 9):2228–39, 2008.

[27] T. Igarashi, C. R. Brown, Y. Endo, A. Buckler-White, R. Plishka, N. Bischofberger, V. Hirsch, and M. A. Martin. Macrophage are the principal reservoir and sustain high virus loads in rhesus macaques after the depletion of CD4+ T cells by a highly pathogenic simian immunodeficiency virus/HIV type 1 chimera (SHIV): Implications for HIV-1 infections of humans. *Proc Natl Acad Sci U S A*, 98(2):658–63, 2001.

[28] A. Iwasaki. Mucosal dendritic cells. *Annual Review of Immunology*, 25:381–418, 2007.

[29] C.A Janeway, P. Travers, M. Walport, and M. Shlomchik. *Immunobiology: The immune system in health and disease*. Garland Publishing, 5 edition, 2001.

[30] L.E. Jones and A.S. Perelson. Modeling the effects of vaccination on chronically infected HIV-positive patients. *Journal of Acquired Immune Deficiency*, 6:369–377, 2002.

[31] S. M. Kaech and R. Ahmed. Immunology: CD8 T cells remember with a little help. *Science*, 300(5617):263–5, 2003.

[32] A. T. Kamath, S. Henri, F. Battye, D. F. Tough, and K. Shortman. Developmental kinetics and lifespan of dendritic cells in mouse lymphoid organs. *Blood*, 100(5):1734–1741, 2002.

[33] I. Karlsson, B. Malleret, P. Brochard, B. Delache, J. Calvo, R. Le Grand, and B. Vaslin. Dynamics of T-cell responses and memory T cells during primary simian immunodeficiency virus infection in cynomolgus macaques. *J Virol*, 81(24):13456–68, 2007.

[34] A. L. Kinter, R. Horak, M. Sion, L. Riggin, J. McNally, Y. Lin, R. Jackson, A. O'Shea, G. Roby, C. Kovacs, M. Connors, S. A. Migueles, and A. S. Fauci. CD25+ regulatory T cells isolated from HIV-infected individuals suppress the cytolytic and nonlytic antiviral activity of HIV-specific CD8+ T cells in vitro. *AIDS Res Hum Retroviruses*, 23(3):438–50, 2007.

[35] D. Kirschner. Dynamics of co-infection with M. tuberculosis and HIV-1. *Theoretical Population Biology*, 55:94–109, 1999.

[36] D.E. Kirschner and G.F. Webb. Immunotherapy on HIV-1 infection. *Journal of Biological Systems*, 6:71–83, 1998.

[37] C. Kornfeld, M. J. Ploquin, I. Pandrea, A. Faye, R. Onanga, C. Apetrei, V. Poaty-Mavoungou, P. Rouquet, J. Estaquier, L. Mortara, J. F. Desoutter, C. Butor,

R. Le Grand, P. Roques, F. Simon, F. Barre-Sinoussi, O. M. Diop, and M. C. Muller-Trutwin. Antiinflammatory profiles during primary SIV infection in African green monkeys are associated with protection against AIDS. *J Clin Invest*, 115(4):1082–91, 2005.

[38] A. Lanzavecchia and F. Sallusto. Regulation of T cell immunity by dendritic cells. *Cell*, 106(3):263–6, 2001.

[39] Q. Li, J. D. Estes, P. M. Schlievert, L. Duan, A. J. Brosnahan, P. J. Southern, C. S. Reilly, M. L. Peterson, N. Schultz-Darken, K. G. Brunner, K. R. Nephew, S. Pambuccian, J. D. Lifson, J. V. Carlis, and A. T. Haase. Glycerol monolaurate prevents mucosal SIV transmission. *Nature*, 2009.

[40] S. Li, E. J. Gowans, C. Chougnet, M. Plebanski, and U. Dittmer. Natural regulatory t cells and persistent viral infection. *J Virol*, 82(1):21–30, 2008.

[41] V. Marechal, M. C. Prevost, C. Petit, E. Perret, J. M. Heard, and O. Schwartz. Human immunodeficiency virus type 1 entry into macrophages mediated by macropinocytosis. *J Virol*, 75(22):11166–77, 2001.

[42] A. L. Marzo, K. D. Klonowski, A. Le Bon, P. Borrow, D. F. Tough, and L. Lefrancois. Initial T cell frequency dictates memory CD8+ T cell lineage commitment. *Nat Immunol*, 6(8):793–9, 2005.

[43] A.R. McLean and T.B.L. Kirkwood. A model of human immunodeficiency virus infection in T helper cell clones. *J. Theor. Biol.*, 147:177–203, 1990.

[44] A.R. McLean and M.A. Nowak. Models of interactions between HIV and other pathogens. *J. Theor. Biol.*, 155:69–102, 1992.

[45] S. R. Mikkelsen, J. M. Long, L. Zhang, E. R. Galemore, S. VandeWoude, and G. Dean. Regulatory T cell depletion prior to acute feline immunodeficiency virus infection does not alter disease pathogenesis. *PLoS ONE*, Submitted.

[46] S. R. Mikkelsen, S. K. Reckling, E. A. Egan, and G. A. Dean. In vivo depletion of CD4(+)CD25(hi) regulatory T cells is associated with improved antiviral responses in cats chronically infected with feline immunodeficiency virus. *Virology*, 403(2):163–72, 2010.

[47] C. J. Miller, Q. Li, K. Abel, E. Y. Kim, Z. M. Ma, S. Wietgrefe, L. La Franco-Scheuch, L. Compton, L. Duan, M. D. Shore, M. Zupancic, M. Busch, J. Carlis, S. Wolinsky, and A. T. Haase. Propagation and dissemination of infection after vaginal transmission of simian immunodeficiency virus. *J Virol*, 79(14):9217–27, 2005.

[48] Y. Onishi, Z. Fehervari, T. Yamaguchi, and S. Sakaguchi. Foxp3(+) natural regulatory T cells preferentially form aggregates on dendritic cells in vitro and actively inhibit their maturation. *Proceedings of the National Academy of Sciences of the United States of America*, 105(29):10113–10118, 2008.

[49] K. Oswald-Richter, S. M. Grill, N. Shariat, M. Leelawong, M. S. Sundrud, D. W. Haas, and D. Unutmaz. Hiv infection of naturally occurring and genetically reprogrammed human regulatory t-cells. *PLoS Biol*, 2(7):E198, 2004.

[50] G.A.F. Seber and C.J. Wild. *Nonlinear Regression*. Wiley, 1989.

[51] E. M. Shevach. Mechanisms of foxp3+ t regulatory cell-mediated suppression. *Immunity*, 30(5):636–45, 2009.

[52] N. Singh, M. Yamamoto, M. Takami, Y. Seki, M. Takezaki, A. L. Mellor, and M. Iwashima. CD4(+)CD25(+) regulatory T cells resist a novel form of CD28- and Fas-dependent p53-induced T cell apoptosis. *J Immunol*, 184(1):94–104, 2010.

[53] S. Stoll, J. Delon, T. M. Brotz, and R. N. Germain. Dynamic imaging of T cell-dendritic cell interactions in lymph nodes. *Science*, 296(5574):1873–6, 2002.

[54] A. M. Thornton and E. M. Shevach. Suppressor effector function of cd4(+)cd25(+) immunoregulatory t cells is antigen nonspecific. *Journal of Immunology*, 164(1):183–190, 2000.

[55] U. H. von Andrian and T. R. Mempel. Homing and cellular traffic in lymph nodes. *Nature Reviews Immunology*, 3(11):867–878, 2003.

[56] B. D. Walker and D. R. Burton. Toward an AIDS vaccine. *Science*, 320(5877):760–4, 2008.

[57] L. S. Walker, A. Chodos, M. Eggena, H. Dooms, and A. K. Abbas. Antigen-dependent proliferation of CD4+ CD25+ regulatory T cells in vivo. *J Exp Med*, 198(2):249–58, 2003.

[58] D. Xiao and W.H. Bossert. An intra-host mathematical model on interaction between HIV and Malaria. *Bulletin of Mathematical Biology*, 72:1892–1911, 2010.

A   Initial Conditions, Parameters and Rate Functions

Initial variable concentrations are given in Table 6. In general, subscripts denote phenotype.

Table 6: Initial conditions.

D_i	Immature dendritic cells	10^8 cells/mL [26]
D^I	Non-infected active dendritic cells in the GLN	10^{-10} cells/mL
D^{I*}	Infected active dendritic cells in the GLN	1 cells/mL
D^E	Non-infected active dendritic cells in the LP	10^{-10} cells/mL
D^{E*}	Infected active dendritic cells in the LP	10 cells/mL
T_m	Non-infected CD4+ memory T-cells	10^8 cells/mL [23]
T_m^*	Latently infected CD4+ Memory T-cells	10^{-10} cells/mL
T^I	Non-infected active CD4+ Th1 cells in the GLN	10^{-10} cells/mL
T^{I*}	Infected active CD4+ Th1 cells in the GLN	1 cells/mL
T^E	Non-infected active CD4+ Th1 cells in the LP	10^{-10} cells/mL
T^{E*}	Infected active CD4+ Th1 cells in the LP	10 cells/mL
R_m	Non-infected memory CD4+ nTreg cells	10^7 cells/mL [7]
R_m^*	Latently infected memory CD4+ nTreg cells	10^{-10} cells/mL
R^I	Non-infected active CD4+ nTreg cells in the GLN	10^{-10} cells/mL
R^{I*}	Infected active CD4+ nTreg cells in the GLN	1 cells/mL
R^E	Non-infected active CD4+ nTreg cells in the LP	10^{-10} cells/mL
R^{E*}	Infected active CD4+ nTreg cells in the LP	10 cells/mL

The alphanumeric superscript denotes location and the superscript '*' indicates infectious counterpart.

Parameters required by the model are listed in Table 7 and fall roughly into three categories: i) birth/death processes, ii) migration, and iii) contact/interaction processes. Units for rates are per 6 hours as this is approximately the length of time a T-cell takes to proliferate in association with the stimulating DC [53]. When possible, constant values were assigned according to published experimental data. For example, p_{t0}, the uninhibited rate of T-cell proliferation in the GLN, is based on an *in vitro* study of CD8+ T-cells and their capacity to proliferate in response to TCR stimulation [21]. This study reported that a stimulated naive CD8+ T-cell or central memory T-cell undergoes a maximum of 9 doublings. Hence 1 T-cell will end-up giving birth to $2^9 = 512$ T-cells. The parameter p_{T0}, the uninhibited rate of T-cell proliferation in the LP comes from observations in the same study that, upon stimulation, effector memory T-cells proliferate to a lower extent than do central memory T-cells resulting in a concentration ratio of roughly 1:4. Proliferation of naive nTreg may be reduced compared to T-helper cells as the express lower levels of IL2R [57]. For this reason, p_r was included as a separate parameter assigned the range 128-512. By default,

Table 7: Parameters used in the model. The third column is for the values of the parameters used in the simulations, and the fourth column is for the ranges of those parameters whose ranges can be found in the literature. For those parameters whose values can not be found in the literature an arbitrary value was assigned. While for those parameters whose values or ranges can be found in the literature, the reference numbers were given after the values or ranges, and the species from which *in vivo* these measurements were taken or cells were isolated for measurements *in vitro* were indicated after the reference numbers with "M" for "mouse", "H" for "human", and "NS" for "not specified".

Birth/death

μ_T	rate of active T-cell deactivation	$0.05/6hr$ [42, M]	
p_{t0}	number of daughter cells from one proliferating T-cell in the GLN, uninhibited	512 [21, H]	
p_{T0}	number of daughter cells from one proliferating T-cell in the LP, uninhibited	128 [21, H]	
μ_{di}	death rate of immature dendritic cells	$0.0006/6hr$ [32, M]	
μ_d	death rate of dendritic cells	$0.12/6hr$ [38, NS]	
d_0	baseline number of immature dendritic cells	10^8 cells/mL [26, NS]	
p_r	number of daughter cells from one proliferating naive CD4+ nTreg	512	
N_E	number of free virus produced by one T-cell	200	$100 - 300$ [25, 29, 19, H]
N_D	number of free virus produced by one DC	5	
c_{NK}	the maximum value of μ_{NK}	$75/6hr$	
λ	the rate at which μ_{NK} rises to its maximum	10^{-8} mL/cells	
m	coefficient to determine effect of CD4+ nTreg on Th1 proliferation	10^{-10} mL/cells	

Migration

ε_{IE}	rate of cell migration from GLN to LP	$0.125/6hr$ [29, NS]	
ε_{EI}	rate of cell migration from LP to GLN	$0.25/6hr$	
ε_t	Number of naive T-cells recruited by one active DC	100	$100 - 300$ [53, M]
c_m	constant in ε_m function	1 cells/(mL·$6hr$)	

Contact / interactions

α_t	probability of naive T-cell stimulation by DC	10^{-4}	$10^{-4} - 10^{-7}$ [29, NS]
α_T	probability of memory T-cell stimulation	10^{-4}	$10^{-5} - 10^{-3}$ [29, NS]
ν_T	fraction of T-cells that become memory T-cells	0.02	$0.02 - 0.1$ [31, M]
δ	fraction of D^* able to stimulate resting T-cells	1	
δ_r	fraction of D^* able to stimulate resting nTreg	1	
α_v	probability of memory T-cell infection by virus on contact	0.1	
α_m	probability of viral infection of D_i upon uptake of virion	0.01	$0.01 - 0.5$ [41, H]
k	rate of contact between individuals	10^{-7} mL/(cells·$6hr$)	
k_T	rate of contact between CD4+ nTreg and DC	10^{-6} mL/(cells·$6hr$)	$(10^{-9} - 10^{-3})$ [48, M]

we assumed that naive nTreg proliferate to the same extent as naive T-helper cells.

The range for ε_t was derived based on the observation of Stoll et al., [53] that there are 3.35 times more naive T-cells in the lymph nodes with presenting dendritic cells compared to lymph nodes where they are absent. As the concentration of naive T-cells in lymphoid tissue in non-inflammatory conditions is on the order of 10^8 [23] this would require an increase of approximately $2 \cdot 10^8$ naive T-cells under inflammatory conditions for a total of approximately $3 \cdot 10^8$. Given that the expected number of activated dendritic cells under inflammatory conditions is approximately 10^6 in the LN [18], one dendritic cell is estimated to recruit approximately $2 \cdot 10^2$ T-cells, giving ε_t a range of 10^2 to $3 \cdot 10^2$.

The parameter d_0 represents the number of immature DC in the naive system. The value assigned was borrowed from a previously published model [26], though an experimental measurement was not cited.

For transition rates such as death, de-activation, and migration rates: μ_T, μ_{di}, μ_d, ε_{IE}, and ε_{EI}, measurements from the literature were in the form of an average lifespan or dwell time for an individual cell type in a particular location. In order to avoid introducing the complication of delay-differential equations, we used the common strategy of modeling cell death and movement as affecting a fixed proportion of cells in each time interval, resulting in an exponential distribution of lifetimes with the experimentally observed mean, x, or a half-life of $x \ln 2$.

For other parameters such direct data was not found and a range was estimated based on less direct biological measurements and knowledge. In the case of α_m, it is not known with what frequency viable virions are able to escape the intra-cellular phagosomal degradation and enter the cytoplasm to effectively infect the dendritic cell. Therefore, we assigned a range based on the ratio of viral protein p24 in the cytoplasm to that in the phagosome after uptake by macrophages [41]. However, p24 is a marker of the virion capsule, not necessarily an intact, viable virion. In the case of α_v, the probability that a resting memory T-cell in infected upon contact with virus, a value was assigned based on the knowledge that the viral receptor protein CD4 is upregulated only in active T-cells and present at lower levels on the surface of resting cells [29]. However, a quantitative comparison of CD4 density between resting and active T-cells was not found in the literature.

The parameter N_E represents the amount of viable virus budded from T-cells. Viral burst size in T-cells is approximately 1100 virions/cell per day *in vitro* [29]. However, only 10% of virus produced is estimated to be viable *in vivo* [19]. Hence, the amount of viable virus produced by a single T-cell is estimated to be on the order to 10^2 per day. N_D represents the amount of virus budded from each dendritic cell. This is known to be less than that of T-cells and the value is assigned based on data that the burst size in macrophages, cells

of the same lineage as dendritic cells, is roughly 0.1 that of the burst size in T-cells [27].

In the case where the quantitative value of a parameter does not have a direct correlation with experimental data, as in the cases of c_{NK}, λ, m, k, k_T, and c_m, a value was arbitrarily chosen.

The parameter dependent rate functions are summarized in Table 8.

Table 8: Parameter dependent rate functions.

Birth/death

Death rate of infected cells by NK: $\mu_{NK} = c_{NK}(1 - e^{-\lambda(D^E + \delta D^{E*} + T^E + T^{E*})})$

Daughter cells produced from one proliferating T-cell in the GLN, inhibited: $p_t = \dfrac{p_{t0}}{1 + m(R^I + R^{I*})}$

Daughter cells produced from one proliferating T-cell in the LP, inhibited: $p_T = \dfrac{p_{T0}}{1 + m(R^E + R^{E*})}$

Migration

Recruitment rate of D_i by inflammatory factors: $\varepsilon_m = c_m \dfrac{T^{E*} + D^{E*}}{T^{E*} + D^{E*} + R^E}$

Contact / interactions

Rate of infection of memory T-cells: $\omega_1 = k\alpha_v(v_E + v_I)$

Rate of contact with virus in the LP: $\omega_2 = kv_E$

Rate of contact with virus in the GLN: $\omega_3 = kv_I$

The concentration of free virus in the LP: $v_E = N_E(T^{E*} + R^{E*}) + N_D D^{E*}$

The concentration of free virus in the GLN: $v_I = N_E(T^{I*} + R^{I*}) + N_D D^{I*}$

B Simplifying Assumptions

B.1 Changes From Earlier Model and Rationale

This model is a result of iterative attempts at reducing an earlier, more comprehensive model. That model was more biologically accurate at the expense of being intractably complex. In this section we list the simplifying assumptions made in the reduction process.

- *No non-HIV antigen, L:* In order to observe potential effects of a co-infecting or previous infection with an inflammatory or tolerance-inducing immunogen previous versions of the model included a variable L representing non-HIV antigen. An explicit variable was not deemed necessary as these effects may be represented, instead, by modification of the initial values of active immune cell populations. In the case of a constant supply of a tolerance-inducing antigen, it may be necessary to include a 'source' parameter for D^E and then reflect the likelihood of it being of a tolerogenic phenotype in the α_T and α_t parameters.

- *Do not consider pre-integrated virus in the latently infected memory T-cell population:* In earlier versions, the latently infected T-cell population was divided into those with integrated virus (T_m^*) and those with pre-integrated virus (I^*). This model does not distinguish the I^* and T_m^* populations. This assumption is made given the short time frame of interest (2 weeks) and fact that the cell takes approximately 1 week to degrade pre-integrated virus. We assume that all memory cells that are infected will be stimulated before virus is degraded.

  Hence, the current model allows T-cells an extra week to be stimulated which may overestimate the prevalence of infected T-cells. To incorporate the fact that some may not be stimulated within a week, and revert back to a non-infected memory T-cell, one could replace α_v with $(\alpha_v - \nu_{T*})$, where ν_{T*} is the probability of reversion back to an uninfected T_m upon viral degradation.

  The insignificance of this effect is supported by the relatively low sensitivity of viral proliferation to the parameter α_v in the sensitivity analysis.

- *No macrophages:* In earlier versions macrophages were included as variables and specifically played a role in: i) stimulation and infection of resting T-cells, ii) virus production, and iii) recruitment of D_i. Excluding macrophages follows the biological model that T-cell stimulation occurs primarily through dendritic cells and viral production by macrophages is only significant in their role as a reservoir in chronic infection, not acute infection.

  The mechanism in which they might have a significant impact is in recruitment: nTreg mediated regulation may occur through promoting the differentiation of M1

to M2 where M1 can recruit and lead to higher D_i levels and M2 does not. This macrophage-mediated recruitment is included as ε_m in Equation (1) to promote a net increase in D_i under inflammatory conditions. The lack of induced T-regulatory cells may skew recruitment dynamics, however sensitivity analysis did not show c_m to be highly influential.

- *Only effector, inflammatory T-cells are included:* This version does not include induced T-regulatory cells (iTreg), but rather only inflammatory Th1 cells. To distinguish iTreg and Th1 is not necessary as CD4+ T-cells are merely included as virus producers. Representing only T-cells of the Th1 phenotype allows us to model the response to the virus, specifically, which is generally Th1 response [29]. It also allows us to make IFN-γ-dependent functions (NK activity and viral production rate) dependent directly on T-cell concentration.

  The assumption that virus induces a Th1 response is supported by SIV studies that show elevated tissue levels of IFN-γ and IL-12 following infection [2] and the paradigm that this is the response to intracellular pathogens in general [29].

  A potentially important aspect this simplification may exclude is that infected dendritic cells may induce conventional T-cells to an iTreg phenotype [22], thereby, creating a virus-producing population that does *not* promote an antiviral response. An attempt to include this dynamic is the option to allow infected dendritic cells to still stimulate members of the R_m population, by setting $\delta_r > 0$, but not conventional T-cells, $\delta = 0$. As δ represents inflammatory function of DCs including stimulation of T-cells to a Th1 phenotype as well as recruitment of T-cells to the lymph node, this is also a coefficient for recruitment of resting nTreg by infected D^{I*} in equations (19) and (20).

B.2   The Assumptions That May Need to Be Re-visited

Below is a list of simplifying assumptions that violate the currently accepted biological understanding of the system and its response.

1. Homeostatic turnover of memory T-cells: The effect of homeostatic cytokine-mediated stimulation of effector and central memory T-cells are not included in the model at this point as it does not appear to play a role in sequence of events in acute infection.

2. Memory T-cells are not currently infected upon transient association with virus-harboring dendritic cells in the absence of antigen recognition.

3. The model assumes that effector functions (cytokine secretion and signalling) is not affected by infection state of a cell.

4. Though the viral life cycle requires approximately 24 hours between infection and budding of nascent virions, the model assumes budding to occur immediately upon infection. Given that this is roughly the time it takes for dendritic cells to migrate from the LP to the GLN upon viral uptake, one could argue that this assumption could lead to a pre-mature spike in free virus concentration in the LP. However, a spike in the LP prior to a spike seen in the GLN actually would agree with viral load curves taken from these tissue areas in an SIV model [47]. Future versions of the model may include a delay term for viral budding from T-cells and DC to capture any possible impact of this 24 hour delay on infection dynamics.

5. The model does not include CTL-mediated removal as a function of T-cells because this would not take place within the scope of two weeks. The time-frame places focus on innate immune aspects.

6. NK cell cytotoxic behavior is promoted by IL-12, IL-15, IL-18, IL-21, IFN-α, and IFN-β *in vitro*. Though *in vivo* studies have linked NK activity specifically with DC-mediated activation, we assume it is dependent on D^E and T^E as Th1 is also a source of IL-12 and IFN.

7. Upon activation T-cells are assumed to proliferate within the first 6 hours, when they actually proliferate after a few days. This may lead to a pre-mature spike in the T-cell population in response to pathogen. Future versions may include a delay term for proliferation to account for any potential impact this may have on T-cell and, therefore, viral dynamics.

8. Through removal of dendritic cells by nTreg the model assumes that anergic dendritic cells do not secrete IL-12, 15, 18, 21, nor IFN-ab that induce NK activity.

9. We assume dendritic cell function is only affected by its infection state and not the cytokine environment.

10. We do not take HIV-induced apoptosis of bystander cells into account under the association of this function with CXCR4 strains and we are modeling CCR5 strains, the most common infecting phenotype. Inclusion of this may have an effect on dynamics placing less emphasis on μ_{NK} for cell depletion.

11. It has been observed that the majority of stimulated mucosal dendritic cells secrete anti-inflammatory IL-10 and TGFβ cytokines [28] upon stimulation by antigen compared to peripheral dendritic cells and, therefore, would not induce a Th1 response. This may warrant modification of the parameters α_T and α_t, the probabilities of conventional T-cell stimulation to an inflammatory Th1 phenotype to incorporate the probability that the presenting dendritic cell is secreting IL-12 as opposed to IL-10/TGF-β.

12. The model assumes that each infected T-cell buds virus at a constant rate over a 1 week activation period as opposed to shedding most virus during its brief proliferation stage.

C   Additional Research Questions Explored

Here are the results from other "low-hanging fruit" experiments that we do not consider highly relevant to the biological community and do not think need to be reported in this study.

C.1   Significance of Infected nTreg Proliferation

It is generally accepted that unlike conventional CD4+ T-cells, memory nTreg do not undergo significant proliferation upon reactivation. However, virus-induced proliferation of latently infected nTreg has been observed *in vitro* in the lab of Dr. Shila Nordone. To test the effect of this proposed proliferation *in vivo* the parameter p_R was included in Equation (20). Simulations were then carried out with a value of $p_R = 512$, representing proliferation of latently infected nTreg upon stimulation.

Preliminary Result Memory nTreg do not proliferate upon re-stimulation by dendritic cells. However, virally-induced proliferation of latently infected nTreg has been observed *in vitro* (unpublished). This hypothesized mechanism is included as the coefficient p_R in Equations (20) and (22). Proliferation is permitted by assigning a value to p_R that is greater than 1. For this reason proliferation of infected memory nTreg, R_m^*, may be included by adding the coefficient p_R to the terms $0.5k\alpha_T R_m^* D^I$ and $0.5k\alpha_T R_m^* D^E$ in Equation (20) and (22). Table 9 shows that whether latently infected nTreg can proliferate upon re-stimulation has a significant impact on the window period for intervention. It may be useful to identify whether this phenomenon occurs *in vitro*, as a potential avenue for intervention.

Table 9: Effect of latently infected nTreg proliferation.

Condition	$\bar{z}_{1max}(t_{peakLP})$	$\bar{z}_{2max}(t_{peakGLN})$
$p_R = 1$	$1.804 \cdot 10^9 (23)$	$5.45 \cdot 10^9\ (26)$
$p_R = 512$	$1.1875 \cdot 10^8 (15)$	$6.7232 \cdot 10^9 (15)$

C.2   Effect of Virus-Induced Inhibition of DC-Mediated nTreg Stimulation

The characteristics of dysfunctional, infected DC described in [22], IL-10 secretion and reduced CD80 expression, may not affect its ability to continue to stimulate nTreg even

when it is unable to induce a Th1 phenotype. One hypothesis states that the evolutionary advantage is found in the inability of DC-mediated NK activity, while at the same time, maintaining DCs ability to stimulate nTreg, which are significant viral producers. To explore this possibility, the model includes δ_r for nTreg stimulation. This is a separate parameter from δ as IL-10 secretion and decreased CD80 levels is sufficient for nTreg stimulation *in vitro* [22]. A $\delta = 0$ and $\delta_r = 1$ represents a scenario in which only inflammatory activity of dendritic cells is compromised where as it is still able to stimulate nTreg. Simulations were run sampling values for these parameter from the set $\{0, 0.74, 1\}$ for δ and $\{0, 1\}$ for δ_r.

Results: Neither affected vRNA levels significantly, with changes being within a factor of 2. The parameter δ did have an impact on the window period, however, as complete inhibition, $\delta = 0$, significantly delays viral propagation of initial viremia and the immune response such that the 'window period' is extended by 3 days in the LP and the GLN, occurring at time points 35 and 37 as opposed to 23 and 26. This is coupled with no significant change in viral load (Table 10).

Table 10: Effect of virus-induced tolerance in DC.

Condition	$\bar{z}_{1max}(t_{peakLP})$	$\bar{z}_{2max}(t_{peakGLN})$
$\delta = 0.74$	$1.804 \cdot 10^9 (23)$	$5.45 \cdot 10^9\ (26)$
$\delta = 0$	$1.7824 \cdot 10^9 (35)$	$5.4317 \cdot 10^9 (37)$

Further analysis: It is possible that allowing infected dendritic cells to stimulate T-cells to proliferating iTreg phenotype would show that these conditions do, indeed, lead to increased viremia. It is possible that allowing infected DC to induce T-cells to proliferating iTreg could have a positive effect on vRNA levels and may be worth exploring in future models in order to contextualize this curious effect on DCs.

Conclusion: This does not support the hypothesis that virus would gain a net benefit in inhibiting DC-mediated inflammation as the decreased μ_{NK} is also coupled with reduced T-cell recruitment and conventional T-cell stimulation. This is true even in the case of continued nTreg stimulation.

C.3   Role of Different Cells in Initial Dissemination

This was tested by reducing the parameters governing infection of resting dendritic cells (α_m) and resting T-cells (α_v) upon contact with virus.

Preliminary results: Reduction of α_v to 10^{-12} had an impact on delaying viral propagation by 1.5 days where as a reduction of α_m to 10^{-12} had a more significant effect in extending the window period by four days, compared to the null model, in both tissues leading with peak levels being reached at time point 44 in the LP and at time point 47 in the GLN, as opposed to time points 23 and 26 (Table 11).

Table 11: Effect of DC and Tm infection

Condition	$\bar{z}_{1max}(t_{peakLP})$	$\bar{z}_{2max}(t_{peakGLN})$
wildtype	$1.804 \cdot 10^9 (23)$	$5.45 \cdot 10^9$ (26)
$\alpha_v = 10^{-12}$	$1.1549 \cdot 10^9 (29)$	$4.2097 \cdot 10^9 (32)$
$\alpha_m = 10^{-12}$	$1.9056 \cdot 10^9 (44)$	$5.6509 \cdot 10^9 (47)$

Conclusions: Infection of dendritic cells is a worthy target of intervention, over inhibiting direct infection of resting T-cells.